Investigation of non-linear dynamics and design of Adaptive Fuzzy Sliding Mode Controller(AFSMC) for Tripod supporter with shape memory alloy(SMA)

A Thesis

Submitted in partial fulfillment of the requirements for the degree of

Masters in Science

by

Yohannes Kewani Gebrewahid

Supervisor: Hailay Kiros(Asst. Prof.)



Department of Mechanical Engineering
Ethiopian Institute of Technology - Mekelle



Acknowledgments

I extend my deepest gratitude to my advisor, **Hailay Kiros**(**Ass. Prof.**), whose guidance, support, and encouragement were invaluable throughout the research process. Your wisdom and expertise have shaped this work in profound ways, and I am grateful for your dedication.

I would also like to acknowledge **Nebyat Gerezgiher**(**Msc.**), IAC chair head, whose insights and collaboration greatly enriched this thesis. Your contributions have been instrumental in the completion of the thesis.

To my family, who have been my unwavering source of love, encouragement, and support: my mother, **Mulunesh Hailu**, my father, **Kewani Gebrewahid**. Your belief in me has been the driving force behind my academic journey, and I am deeply thankful for your sacrifices and endless encouragement.

Last but certainly not least, I want to express my heartfelt appreciation to my girlfriend, **Fkr**. Your love, patience, and unconditional support have sustained me through the challenges of this endeavor.

To all those who have contributed to this journey in ways seen and unseen, thank you. Your support has been invaluable, and I am thankful for the opportunity to undertake this endeavor.

Declaration

Declaration of the Candidate

I hereby declare that this thesis entitled "Investigation of nonlinear dynamics and design of AFSM-C for tripod supporter with SMA" is the result of my own work, unless otherwise acknowledged. I have properly credited and cited all sources from which I have used data, ideas, or words, either verbatim or paraphrased. I also declare that this work has not been submitted for any other degree or award in any university or institution. I understand that any violation of academic integrity, including plagiarism or fabrication, will result in severe consequences, as outlined by the institutional legislation.

Yohannes Kewani
Id no. eitm/pr160451/11

May, 2024

Declaration of the Advisor

This is to certify that the above declaration made by the candidate is correct to the best of my knowledge and the thesis is adequate for the award of the degree of Master of Science in Mechatronics Engineering.

Hailay Kiros(Ass. Prof.)

May, 2024

Abstract

This study examines the complex dynamics of a tripod supporter system with shape memory alloy (SMA) alongside Adaptive Fuzzy Sliding Mode Control (AFSMC). It's motivated by the growing interest in creating smarter SMA systems and aims to understand how these systems behave in different situations. The study also seeks to develop better control methods to handle their complexities and uncertainties. Through detailed computer simulations, the research systematically explores how the system behaves in various phases: martensite, transition, and austenite. Each phase is carefully examined to uncover the intricate dynamics governing the system under different conditions. The research begins with a comprehensive review of existing literature, highlighting gaps in the understanding of the system behaviour under a quasi-periodic complex excitation with three frequency terms and the limitations of traditional control methods, while also showcasing the potential of AFSMC to address these challenges effectively. The system's martensite, transition, and austenite phases, characterized by varying temperatures are explored under damping conditions of $\xi = 0.1$ and $\xi = 1.5$ and for forcing parameter of $\gamma = 0.045$. This investigation unveils phenomena such as chaotic behavior and attracting tori across all phases. Analysis of Lyapunov exponents sheds light on the system's sensitivity to initial conditions and convergence tendencies, while bifurcation simulations consistently indicate the potential for bistability within the system. The study also evaluates the effectiveness of AFSMC across the three phases, showing robust performance in reducing vibrations. Comparative analyses against traditional sliding mode control methods provide compelling evidence of AFSMC's superiority, emphasizing its resilience and adaptability in managing uncertainties. In summary, this study offers a comprehensive exploration of SMA-integrated system dynamics and AFSMC's efficacy in control, providing valuable insights for the broader field of nonlinear control and SMA-based engineering applications.

Keywords: Tripod supporter, SMA, quasi periodic, Chaos, AFSMC

Contents

A	know	ledgme	ents	vii
Al	bstrac	et		xi
Li	st of I	Figures		xvii
Li	st of T	Fables		xix
1	Intr	oductio	n	1
	1.1	Backg	round	. 1
		1.1.1	Shape Memory Alloys	. 2
		1.1.2	Dynamics of tripod supporter and control strategies	. 4
	1.2	Proble	m Statement	. 6
	1.3	Resear	rch Objectives	. 6
		1.3.1	General Objective	. 6
		1.3.2	Specific Objectives	. 7
	1.4	Metho	dology	. 7
	1.5	Scope	and limitations of the thesis	. 10
	1.6	Thesis	Outline	. 10
2	Lite	rature l	Review	11

xiv Contents

	2.1	Tripod	Supporter		11
	2.2	Shape	Memory A	Alloys	12
	2.3	Consti	tutive Mod	lel	13
	2.4	Nonlin	ear Dynar	nics	14
	2.5	Nonlin	ear Contro	ol	19
3	Mat	hematio	al Model	and stability analysis	21
	3.1	Mathe	matical Mo	odel	22
	3.2	Stabili	ty analysis		24
4	Non	-linear :	analysis a	nd AFSMC design	29
	4.1	Dynan	nical analy	sis	29
		4.1.1	Phase Po	rtrait	29
		4.1.2	Bifurcati	on	31
		4.1.3	Lyapuno	v Exponents	31
	4.2	Contro	ller Desig	n	33
		4.2.1	Adaptive	Fuzzy Sliding Mode Control	33
		4.2.2	Controlle	er Performance Assessment Criteria	35
			4.2.2.1	Integral Absolute Error (IAE)	35
			4.2.2.2	Integral Time Absolute Error (ITAE)	37
			4.2.2.3	Integral Square Error (ISE)	37
			4.2.2.4	Undershoot and Overshoot	38
			4.2.2.5	Fall Time	38
5	Resu	ult and	Discussior	n1	39
	5.1	Introdu	action		39
	5.2	Equilib	orium Poin	ats and Their Stability	40

Contents xv

	5.3	Dyanamics in Martensite phase	41			
	5.4	Dynamics in Transition phase	46			
	5.5	Dynamics in Austensite Phase	47			
	5.6	Adaptive Fuzzy Sliding Mode Controller	51			
		5.6.1 Martensite phase	52			
		5.6.2 Transition Phase	54			
		5.6.3 Austenite Phase	56			
6	Con	clusion and Recommendation	59			
	6.1	Conclusion	59			
	6.2	Recommendations	60			
Bi	Bibliography					
Ap	pend	ices	69			
A	Matlab code for calculating and ploting Equilibrium points and Eigenvalue					
В	Mat	lab code for ploting forward and backward continuation Bifurcation diagram	73			
C	Mat	lab code for implementing the adaptive fuzzy system	77			

List of Figures

1.1	Flowchart of the Methodology of the study	ç
3.1	System geometry of the SMA supporter	22
3.2	System simulink Model	24
4.1	Phase Space	30
4.2	Simulink Model for Phase Portrait Simulation	31
4.3	Flowchart for bifurcation diagram simulation	32
4.4	Tripod system with the AFSMC	36
4.5	Adaptive Fuzzy Sliding Mode Controller Simulink Model	36
5.1	Equilibrium Points	40
5.2	Eigenvalues	41
5.3	Phase portrait for $\xi=0.1$	42
5.4	Phase portrait for $\xi=1.5$	42
5.5	Time series for $\xi=0.1$, showing sensitivity to initial conditions $\dots \dots \dots$	43
5.6	Time series for $\xi=1.5$, demonstrating convergence for close initial conditions $\ \ .\ \ .$	44
5.7	Bifurcation diagram for varying γ with $\xi=0.1$	45
5.8	Bifurcation diagram for varying ξ	45
5.9	Phase portrait in transition phase for $\xi = 0.1 \dots \dots \dots \dots$	46

xviii List of Figures

5.10	Phase portrait in transition phase for $\xi = 1.5$	46
5.11	Time series for $\xi=0.1$, showing sensitivity to initial conditions $\dots \dots \dots$	47
5.12	Time series for $\xi = 1.51$, showing convergence to initial conditions	48
5.13	Bifurcation in transition phase for $\xi=0.1$	48
5.14	Phase portrait in Austenite phase for $\xi=0.1$	49
5.15	Phase portrait in Austenite phase for $\xi=1.5$	49
5.16	Time series for $\xi=0.1$, showing sensitivity to initial conditions $\dots\dots\dots$	50
5.17	Time series for $\xi=1.5$, showing convergence to initial conditions	50
5.18	Bifurcation in Austenite phase for $\xi=1.5$	51
5.19	Membership Function for the adaptive fuzzy	52
5.20	Estimation of disturbance using Adaptive Fuzzy System	52
5.21	AFSMC Performance in Martensite Phase	53
5.22	Comparison of AFSMC and SMC in Martensite Phase	53
5.23	AFSMC in Transition Phase	55
5.24	Comparison of AFSMC and SMC in Transition Phase	55
5.25	AFSMC in Austenite Phase	57
5.26	Comparison of AFSMC and SMC in Austenite Phase	57

List of Tables

5.1	AFSMC Controller Performance in Martensite Phase	54
5.2	Comparison of AFSMC and SMC Performance in Martensite Phase	54
5.3	AFSMC Controller Performance in Transition Phase	56
5.4	Comparison of AFSMC and SMC Performance in Transition Phase	56
5.5	AFSMC Controller Performance in Austenite Phase	58
5.6	Comparison of AFSMC and SMC Performance in Austenite Phase	58

1

Introduction

1.1 Background

Shape memory alloys (SMAs) have garnered significant attention in the past few decades due to their unique properties and versatile applications across various fields. These metallic alloys exhibit the remarkable ability to recover their original shape from significant deformations through thermal processing, making them invaluable in engineering applications. The behavior of SMAs, characterized by martensitic phase transformation, presents intriguing challenges and opportunities for researchers and engineers.

In the realm of structural dynamics, the study of systems subjected to multi-frequency excitation

has become a focal point for understanding complex behaviors and responses. The investigation of quasiperiodic excitation with multiple terms offers a deeper insight into the dynamics of systems under intricate stimuli, revealing novel phenomena and interactions. Expanding the research from dual-frequency to tri-frequency excitation introduces a new level of complexity, paving the way for exploring non-linear dynamics.

However, a notable gap in the current literature lies in the application of control strategies to systems under multi-frequency excitation. While existing studies focus on the dynamics and behavior of such systems, the integration of advanced control techniques, such as adaptive fuzzy sliding mode controllers(AFSMC), remains unexplored. The addition of a controller not only enhances the system's stability and robustness but also bridges the gap between theoretical analysis and practical implementation.

Therefore, this thesis aims to address this gap by investigating the dynamics of a three-leg supporter with shape memory alloy under quasiperiodic excitation with three terms and incorporating an AF-SMC for enhanced control and stability. By combining theoretical analysis with practical control strategies, this research seeks to advance our understanding of complex dynamical systems under multi-frequency excitation and contribute to the development of effective control methodologies for engineering applications.

1.1.1 Shape Memory Alloys

Shape memory alloys (SMAs) belong to a category of smart materials with unique properties stemming from changes in their microstructure when exposed to external non-mechanical stimuli, such as variations in temperature. In thermally responsive SMAs, they exhibit reversible solid-solid, diffusionless thermoelastic phase transitions between a stable high-temperature austenitic phase and a low-temperature martensitic phase. These transformations give rise to remarkable phenomena like the shape memory effect (SME) and superelasticity (SE). The SME is the capacity to revert to a predefined shape when heated. Meanwhile, SE refers to their ability to recover significant strains (approximately 8%) and the associated substantial stress-strain hysteresis during mechanical loading

1.1. Background 3

and unloading under isothermal conditions [1].

In 1932, Ölander made the initial observation of the SME, and it was in 1941 that Vernon introduced the term 'shape memory.' Fast forward to 1961, Buehler and Wiley, while conducting research at the US Naval Ordinance Laboratory, identified a group of alloys, specifically Nickel and Titanium, that exhibited the shape-memory phenomenon. Due to a combination of factors, including the alloy's composition and its discovery at the Naval Ordinance Lab, this alloy became known as NiTiNOL (a portmanteau of Nickel, Titanium, and Naval Ordinance Lab). These discoveries have generated considerable interest and extensive research, both in terms of understanding the properties and exploring potential unique applications in various structures [2].

Over the past twenty years, substantial research and development efforts have been dedicated to S-MAs. These endeavors have been propelled by advancements in materials science, improvements in laboratory equipment, the application of advanced computational methods, and various other enhancements. These noteworthy progressions in both research and technology have led to a deeper understanding of phase transformations, streamlined production and utilization processes, and the identification of cost-effective alloys exhibiting shape-memory properties [2]. There has been significant research and experimentation involving laminated composites that incorporate embedded SMA wires. This development has brought forth novel attributes and qualities to the host structures [3]. Cost-effective shape memory alloys based on Fe and Cu are developed to reduce the limitation due to the high cost of manufacturing and installation of NiTinol alloy [2].

SME and related occurrences are rooted in a primary phase shift between a high-temperature phase, typically known as austenite, and a low-temperature phase, often referred to as martensite. The transition from austenite to martensite commences and concludes at specific temperatures, known as the martensite start temperature (Ms) and martensite finish temperature (Mf) [1]. Conversely, temperature transitions from martensite to austenite are termed austenite start temperature (As) and austenite finish temperature (Af). Depending on the stress and temperature conditions concerning these transformation temperatures, various phenomena can be observed: The SME, the two-way shape memory effect (TWSME), and SE. In all instances, alterations are made to operating temperatures and/or applied stresses, while the inherent transformation temperatures of the utilized SMA remain constant

during use [4].

Shape memory alloy characteristics are dependent on the compositions of the alloying materials. The most common compositions of shape memory alloys are the NiTi, copper-based, and ferrium-based alloys. SMAs are a class of materials known for their unique properties, which are attributed to their specific composition.

The NiTi alloy has characteristics in SME, SE that outperform other shape memory alloy types. Nickel (Ni) and titanium (Ti) are the primary composition of binary NiTi shape memory alloy [2]. Nickel is a crucial component in SMAs, typically comprising around 50% to 55% of the alloy by weight. It contributes to the alloy's shape memory effect and superelasticity properties. Nickel-rich regions (austenite phase) of the alloy are responsible for high-temperature stability and flexibility. Titanium accounts for the remaining 45% to 50% of the alloy's composition. It plays a significant role in the low-temperature martensitic phase of the SMA, allowing the alloy to undergo reversible phase transformations and exhibit shape memory properties. The cost of manufacturing and installing NiTi alloy is relatively high, limiting its application to specific areas. Additionally, its high thermal sensitivity makes it unsuitable for systems operating in rapidly changing environments [2].

1.1.2 Dynamics of tripod supporter and control strategies

Expanding the investigation of tripod supporter with SMA from quasiperiodic excitation with two terms to three terms presents an intriguing research gap in the current literature. While existing studies have explored the dynamics and behavior of systems under dual-frequency excitation, the extension to tri-frequency excitation introduces a new level of complexity and richness in the system's response. By incorporating an additional frequency component, the research can delve into the interactions phenomena that arise from the interplay of three distinct frequencies.

Investigating quasiperiodic excitation with three terms offers the opportunity to uncover novel dynamics, such as multi-stability in the whole phases of the system not observable in dual-frequency systems. This extension can provide a more comprehensive understanding of the system's behavior under multi-frequency excitation, offering insights into how the additional frequency component

1.1. Background 5

influences the system's stability, bifurcation scenarios, and chaotic behavior.

Furthermore, exploring the effects of tri-frequency excitation can have practical implications for engineering applications where systems are subjected to complex multi-frequency inputs. Understanding how structures respond to three-frequency excitation can inform the design of more robust and adaptive control strategies tailored to such intricate excitation profiles. Overall, investigating quasiperiodic excitation with three terms fills a significant gap in the current research landscape and opens up new avenues for exploring the dynamics of complex systems under multi-frequency stimuli.

Integrating an AFSMC into the study of a three-leg supporter under quasiperiodic excitation with three terms presents a notable research gap in the existing literature. While the current research focuses on the system's dynamics and response to dual-frequency excitation, the introduction of a controller adds a new dimension by addressing the practical aspect of controlling and stabilizing the system in real-time.

The incorporation of an adaptive fuzzy sliding mode controller offers several advantages, including robustness to uncertainties, disturbances, and variations in the system parameters. By adapting the controller's parameters based on the system's dynamics and input signals, the AFSMC can enhance the system's stability and resilience to external perturbations.

Furthermore, the AFSMC allows for online tuning and adjustment, enabling the system to adapt to changing operating conditions and disturbances effectively. This adaptive control strategy can improve the system's performance under varying excitation profiles and enhance its ability to track desired trajectories while mitigating the effects of nonlinearities and uncertainties inherent in the system.

By incorporating an AFSMC, the research can bridge the gap between theoretical analysis and practical implementation, offering insights into the feasibility and effectiveness of control strategies in real-world applications. Additionally, studying the interaction between the controller and the multi-frequency excitation can provide valuable knowledge on the design and optimization of control systems for complex dynamical systems. Overall, integrating an adaptive fuzzy sliding mode controller represents a significant advancement in the study of multi-frequency-excited tripod system with S-

MA and opens up avenues for enhancing the system's controllability and performance in engineering applications.

1.2 Problem Statement

SMA represent a class of intelligent materials garnering significant interest in contemporary research. Within the realm of SMA applications, the construction of smart systems has emerged as a promising avenue. Specifically, the incorporation of shape memory alloys into a Tripod supporter has potential utility, particularly in aerospace and machining industries, improving the existing tripod supporters. Despite these advancements, there exists a notable gap in the comprehensive exploration of the non-linear dynamics exhibited by shape memory alloy tripod systems for quasi periodic with tri-frequency complex excitation across varying operational conditions.

Efficiently harnessing the intricate nonlinear behaviors inherent in these systems necessitates a thorough understanding, and thus, the control of such nonlinearities becomes imperative. The existing body of literature falls short in addressing the crucial aspect of controlling the nonlinear behavior inherent in the Tripod system integrated with SMA bars. Consequently, this research endeavors to bridge these gap by conducting a rigorous investigation into the nonlinear dynamics for qusi-periodic excitation with three frequency terms and implementing AFSMC for the Tripod supporter, thereby advancing the understanding and practical utilization of smart tripod systems in relevant industrial domains.

1.3 Research Objectives

1.3.1 General Objective

The general objective of this thesis is to investigate the non-linear dynamics and design AFSMC for a tripod supporter with shape memory alloy.

1.4. Methodology 7

1.3.2 Specific Objectives

The specific objectives of this thesis are as follows:

• To develop the mathematical model and analyze the nonlinear dynamic behaviour of the tripod

supporter.

• Design an Adaptive Fuzzy sliding Mode Controller(AFSMC) for the system

• Measure the performance of the AFSMC and compare it with Sliding Mode Controller(SMC)

employing performance matrices such as overshoot, falltime, IAE, ISE.

1.4 Methodology

The investigation of the nonlinear dynamics of the tripod supporter with SMA and the design of its controller involve a systematic and comprehensive approach. This methodology is structured to first establish a constitutive model, followed by the mathematical modeling of the entire system using Newton's second law. Subsequently, the exploration of the nonlinear dynamics includes the use of phase portraits, Lyapunov exponent analysis, basin of attraction simulations, and bifurcation simulations. Additionally, an Adaptive Fuzzy Sliding Mode Controller(AFSMC) is integrated into the system.

1. Constitutive Model: Falk Polynomial

The constitutive model plays a crucial role in capturing the mechanical behavior of the tripod supporter. In this study, the Falk polynomial constitutive model of (1.1) is employed [5]. This model is utilized to characterize the mechanical properties of the tripod supporters SMA materials investigation.

$$\sigma = a_1(T - T_m)\varepsilon - a_2\varepsilon^3 + a_3\varepsilon^5 \tag{1.1}$$

2. Mathematical Modelling: Newton's Second Law

To mathematically represent the dynamics of the tripod supporter with SMA, Newton's second law is applied as in Equation(1.2). The equations derived from this fundamental principle of second law of motion serve as the foundation for understanding the motion and forces within the system. Through a rigorous mathematical analysis, the dynamic equations governing the behavior of the tripod supporter are formulated.

$$\Sigma F = ma \tag{1.2}$$

3. Non-linear Dynamics Analysis

Phase Portrait Analysis: Visualizing the system's behavior is essential for gaining insights into its non-linear dynamics. Phase portraits are constructed to illustrate the trajectory of the system in its state space, providing a qualitative understanding of its behavior under varying conditions.

Lyapunov Exponent Analysis: The Lyapunov exponent, a quantitative measure of the system's sensitivity to initial conditions, is calculated to assess the stability and chaos in the system. This analysis aids in identifying critical points and understanding the long-term behavior of the system.

Bifurcation Simulations: Bifurcation simulations are employed to analyze how the system's behavior changes as a function of control parameters. This investigation helps identify bifurcation points and understand the transition between different dynamical regimes, contributing to a deeper comprehension of the system's complex behavior.

4. Controller Integration

The controllers employed are robust and adaptive control methods. The robust sliding mode controller is integrated with adaptive fuzzy approximator to form an adaptive fuzzy sliding mode controller. The results of this controller are compared with the sliding mode controller. The overall process of the study is summarized by the flowchart shown in Figure (1.1)

1.4. Methodology 9

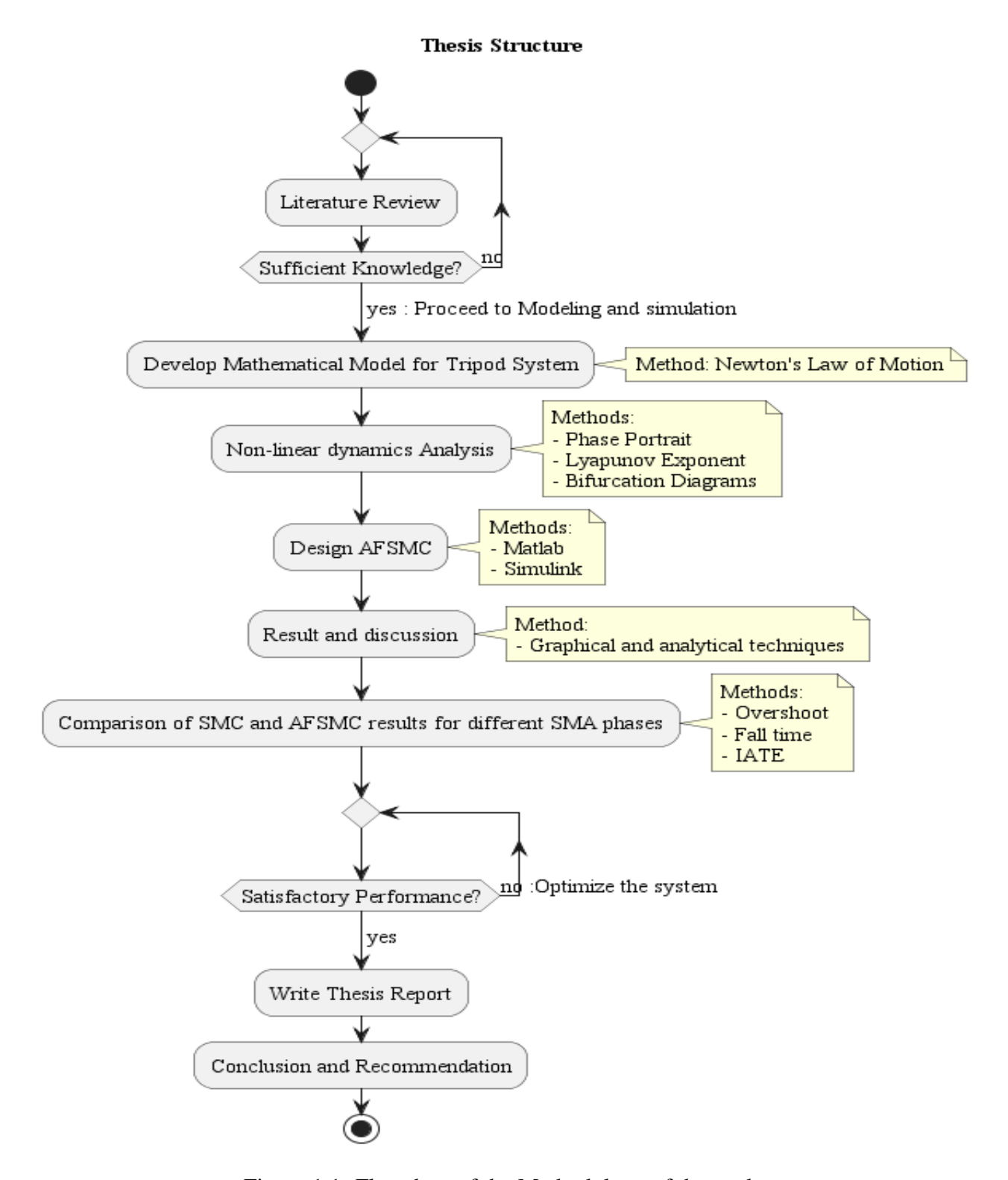


Figure 1.1: Flowchart of the Methodology of the study

1.5 Scope and limitations of the thesis

This research aims to contribute to the understanding of the dynamic behavior of a Tripod supporter with Shape Memory Alloy (SMA) through comprehensive mathematical modeling and simulation-based analyses. The primary focus lies in the mathematical representation of the SMA bars within the supporter, investigating the nonlinear dynamics through simulation techniques, and modeling the application of an Adaptive Fuzzy Sliding Mode controller(AFSMC) under various conditions. The scope encompasses a detailed examination of the system's response, stability, and control strategies to enhance the overall performance.

Due to resource constraints and the nature of the study, experimental tests are not included in the research. The absence of physical experimentation may limit the direct correlation of simulation results to the actual performance of the tripod supporter with SMA in real-world scenarios.

It is important to note that the research activities faced limitations during the Tigrai conflict from 2020 to 2023. The socio-political conditions in the region affected access to certain resources, potentially impacting the comprehensiveness of the study. Efforts have been made to mitigate these limitations, but the potential influence on the study's scope and execution should be acknowledged.

1.6 Thesis Outline

This thesis explores the dynamics of a tripod supporter integrated with shape memory alloy (SMA) and Adaptive Fuzzy Sliding Mode Control (AFSMC). It commences with an Introduction, followed by a comprehensive Literature Review delving into SMA systems and control methods. Chapter 3 presents the mathematical model of the system and its stability analysis methodology. Chapter 4 outlines the methods employed for investigating nonlinear dynamics and AFSMC design. The Results and Discussion chapter presents findings from nonlinear dynamic analysis and controller performance. The final chapter, Conclusion and Recommendations, deals the outcomes and proposes future research directions

2

Literature Review

2.1 Tripod Supporter

Archetypal models serve as prototypes that symbolize broader systems, playing a crucial role in analyzing the stability features of structures [6]. The tripod support structure, a mechanical system utilized across diverse sectors such as aviation and manufacturing [7], is capable of achieving precise motion with adequate inclination. By integrating shape memory bars, it becomes easier to control precise movements and maintain specific positions. Therefore, it is essential to explore and showcase the performance of this tripod support when equipped with a shape memory alloy structure using an archetypal model.

2.2 Shape Memory Alloys

In recent years, researchers have made significant progress in understanding and harnessing the potential of shape memory alloys (SMAs). These materials, such as Ni-Ti and Cu-Zn-Al, exhibit remarkable properties, including a large reversible strain due to superelasticity. New types of alloys that outperform the commercially available NiTi alloy are being researched [8, 9].

Notably, Tanaka [8] described a high-strength shape memory alloy with a superelastic strain exceeding 13%, having tensile strength above 1000 megapascal. This superelastic strain is almost twice the maximum superelastic strain observed in NiTi. Due to its additional high damping capacity, the paper suggests this ferrous polycrystalline shape memory alloy can be employed as a high damping and sensor material.

Canadinc et al. [9] delved into the characteristics of multi-component alloys, focusing on superelasticity and thermal actuation behavior, while introducing the concept of multi-component ultra-high temperature shape memory alloys, opening up new possibilities for SMA applications. It suggests quaternary and quinary alloying to improve the martensitic transformation temperatures. These multi-component SMAs also have demonstrated good superelastic behavior.

The shape memory effect might be degraded due to the machining process. Thus, it is important to appropriately choose a machining process for SMAs. Chaudhari [10] explored optimization techniques for preserving the shape memory effect during the machining process, which could significantly expand SMA applications. The modified process produced an SMA with a shape memory effect similar to the original material.

Furthermore, T. Wheeler et al. [11] from the Consortium for the Advancement of Shape Memory Alloy Research and Technology has been dedicated to enabling revolutionary applications based on SMA technology by providing best practices and design tools. It developed a modeling framework for three frequently applied SMA actuators.

Recent breakthroughs have expanded the scope of SMA applications. Xia et al. [12] introduced an iron-based superelastic alloy system with optimized critical stress. Compared with NiTi, this iron-

2.3. Constitutive Model 13

based SMA has a low cost and improved cold workability. Costanza [13] reviewed SMA applications in the aerospace field, emphasizing their added value beyond economic benefits. In the field of additive manufacturing, Lu et al. [14] highlighted the enhanced mechanical and shape memory properties of TiNi using heat treatment homogenization.

Pushin et al.[15] explored copper-based shape memory alloys with commercial potential, finding high strength and plasticity, as well as a high shape memory effect. Shen et al.[16] established a simulation model for SMA actuator motion, while Terrile et al.[17] presented a real robot actuated with SMA springs, optimizing its performance using finite elements and neural networks.

In various fields, including automotive and aerospace, researchers are exploring innovative applications of SMAs. Liu et al.[18] addressed challenges in tracking control in SMA-actuated systems, while Turabimana et al.[19] proposed an active engine cooling system utilizing SMA-based thermostat. In the pursuit of high-temperature shape memory alloys, Gomez et al.[20] investigated the thermal stability of Cu-Al-Ni shape memory alloy thin films suitable for technologies operating at elevated temperatures.

The evolving research landscape in the field of shape memory alloys demonstrates their broad applicability, complex properties, and the importance of understanding and studying them for various technological advancements.

2.3 Constitutive Model

Researchers have long been engaged in developing comprehensive constitutive models for shape memory alloys (SMAs). These models are crucial for accurately describing the complex thermomechanical behavior of SMAs under various loading conditions.

Brinson[21] compared and simplified popular SMA constitutive models, emphasizing that the distinction between these models lies primarily in the formulation of the transformation kinetics. Furthermore, Paiva[22] proposed a constitutive model for SMAs that considers both tensile-compressive asymmetry and plastic strains in their thermomechanical behavior. Bahrami[23] delved into frac-

ture investigations and proposed a constitutive model to explore the pseudoelastic-plastic behavior of SMAs up to fracture, drawing from phase transformation models and the Gurson-Tvergaard-Needleman (GTN) model.

Recent research in the last five years has brought forth new advancements in constitutive models for SMAs. Yu et al.[24] introduced a crystal plasticity-based constitutive model for NiTi SMAs, considering various mechanisms of inelastic deformation and extending the single crystal model to a polycrystalline version. They focused on modeling the martensite reorientation and zero/negative thermal expansion in shape memory alloys, introducing a microstructure-based theoretical model with non-linear constitutive aspects. Mostofizadeh et al.[26] implemented one-dimensional thermomechanical constitutive equations into the self-heating method to study fatigue of SMAs efficiently. Furthermore, Phillips et al.[27] incorporated non-linear internal damage growth into an SMA constitutive model, which proved effective for lifetime predictions under various loading conditions.

While simple constitutive models provide an initial understanding of SMA behavior and can be computationally efficient, complex models offer more detailed insights and accuracy, especially when capturing the intricate thermomechanical responses of SMAs under diverse loading scenarios. The choice between simple and complex methods depends on the specific requirements of the study, balancing computational cost with the need for accuracy and comprehensiveness.

The constitutive models employed in SMA research play a crucial role in accurately describing their thermomechanical behavior. Both simple and complex models contribute to advancing our understanding of SMAs and are essential tools for various engineering applications.

2.4 Nonlinear Dynamics

The investigation of non-linear dynamics of a structure is important for application and control of the structure. Kiros[28] discusses the significance of analyzing nonlinear dynamic structures and the use of MATLAB simulations based on two types of nonlinear FRF construction methods, namely Harmonic Balance and Multiple Input Multiple Output (MIMO) or Multiple Input Single Output

(MISO) techniques. The limit of chaos is also determined, and good results are achieved and verified using harmonic balance and FRF. The paper concludes by discussing the practical applications of determining the limit of chaos in nonlinear systems.

Investigating the bifurcation and Lyapunov exponents of a structure is crucial for understanding its dynamic behavior and stability. Bifurcation analysis helps in identifying regions of bistability, where the system exhibits multiple stable states, providing insights into how the system responds to varying parameters. On the other hand, analyzing Lyapunov exponents quantifies the system's chaotic nature and sensitivity to initial conditions. Positive Lyapunov exponents indicate chaotic behavior, while negative values suggest stability. This information is essential for predicting long-term system behavior, optimizing design, developing effective control strategies, and enhancing performance. By studying bifurcation and Lyapunov exponents, researchers can gain a comprehensive understanding of the system's dynamics, enabling them to make informed decisions for design, control, and prediction in engineering applications[7].

In the study by Rajagopal et al. [29] on multistability in Horizontal Platform Systems (HPS) with and without time delays, numerical simulations were employed to simulate bifurcation diagrams and calculate Lyapunov exponents. For the bifurcation diagram simulation, the authors utilized a method where they varied a specific parameter, such as the forcing parameter h within the range of 9.8 to 12.2, and plotted the local maxima of the coordinate x_2 . This approach, known as forward and backward continuation, allowed them to identify regions of multistability by comparing forward and backward bifurcation diagrams.

To simulate the bifurcation diagram, De Paula et al. [30] explored the system's behavior through numerical simulations using a fourth-order Runge–Kutta method with linear interpolation on the delayed variables. This numerical approach allows for the visualization of bifurcation patterns and transitions in the system's dynamics as control parameters are varied, providing insights into the system's response to different conditions.

The simulation of the bifurcation diagram in the study by De Paula et al. [31] was conducted using an iterative numerical procedure based on the operator split technique, the orthogonal projection algorithm, and the classical fourth-order Runge–Kutta method. This approach allowed for a detailed

analysis of the system's dynamic behavior, enabling the researchers to explore the effects of parameter variations and control strategies on the stability and chaotic characteristics of the SMA two-bar truss system.

The method employed by Bessa et al. [6] to simulate the bifurcation diagram involves varying the forcing parameter γ while keeping other parameters such as frequency Ω and damping parameter ξ constant. By systematically changing the value of γ and observing the corresponding behavior of the system, the researchers were able to analyze the response of the shape memory two-bar truss under different conditions, identifying points where the system transitions between different types of behavior.

Huang et al. [32] generated bifurcation diagrams by plotting stroboscopically sampled displacement values under a slow quasi-static increase of the driving force amplitude, considering different dissipation, temperature, and frequency parameters to explore the system's responses, including periodic, quasi-periodic, and chaotic behaviors.

Varadharajan et al. [7] analyzed system for the property of bistability to simulate the bifurcation diagram. They performed a bifurcation analysis to understand the existence of bistability in mechanical systems, employing a technique known as forward and backward continuation. This method provided a systematic way to analyze the bifurcation behavior of the system and identify the presence of bistability, crucial for understanding the complex dynamics of mechanical systems.

In calculating the Lyapunov exponents, Rajagopal et al. [29] adopted a technique involving the synchronization of identical systems coupled by a linear negative feedback mechanism. This method enabled them to determine the exact Lyapunov exponents, which were crucial for assessing the chaotic behavior and stability of the system. The Lyapunov exponents were calculated as $\lambda_1 = 0.2311$ and $\lambda_2 = -1.5245$ for the Time Delayed Horizontal Platform System (TDHPS).

The method employed by Danca et al. [33] to simulate the Lyapunov exponent for fractional-order systems involves modeling the system using Caputo's derivative, constructing an extended system with the initial value problem and variational system, and utilizing the predictor-corrector Adams–Bashforth–Moulton method for numerical integration. This method provides insights into

the average rate of divergence or convergence of orbits in fractional-order systems, aiding in understanding system behavior and stability.

The calculation of Lyapunov exponents by De et al. [30] involves approximating the continuous evolution of the infinite-dimensional system by a finite number of elements where values change at discrete time steps. This approximation allows for the determination of the largest Lyapunov exponent, which is crucial for stability analysis of unstable periodic orbits in the system.

Bessa et al. [6] calculated the Lyapunov exponent to quantify the sensitivity to initial conditions and determine the presence of chaos in the system. By computing the Lyapunov exponent, the researchers were able to assess the rate at which nearby trajectories in phase space diverge or converge.

De et al. [31] utilized an iterative numerical procedure integrating the operator split technique, the orthogonal projection algorithm, and the classical fourth-order Runge–Kutta method to simulate the Lyapunov exponent. This comprehensive approach facilitated a detailed investigation of the Lyapunov exponents and their role in understanding the chaotic dynamics and control mechanisms of the SMA two-bar truss system.

Huang et al. [32] utilized Wolf's algorithm to estimate the Lyapunov exponents, characterizing the system's sensitivity to initial conditions by quantifying the exponential divergence of nearby orbits. The signs of the Lyapunov exponents provide insights into the system's dynamics, with positive exponents indicating chaotic behavior.

Varadharajan et al. [7] employed Wolf's algorithm to simulate the Lyapunov exponent, providing a quantitative measure of the system's chaotic behavior and valuable insights into its dynamics and stability.

The findings from the bifurcation and Lyapunov exponent analyses in the study by A. Savi[6] provided crucial insights into the dynamic behavior of the shape memory two-bar truss. The bifurcation analysis revealed the system's response to varying the parameter γ , showcasing transitions between periodic and chaotic motion at different values. Furthermore, the computation of the Lyapunov exponent offered a quantitative measure of the system's sensitivity to initial conditions and the presence of chaos. Overall, these discoveries not only validated the complex nature of the smart structure but also

underscored the importance of considering nonlinear dynamics and chaos in the design and control of such systems.

The investigations conducted by de. Paula[31] shed light on the dynamic behavior and stability characteristics of the SMA two-bar truss system. By iteratively analyzing the bifurcation diagram, the researchers observed the system's response to varying forcing parameters and control actions, high-lighting the effectiveness of the time-delayed feedback control method in stabilizing unstable periodic orbits and avoiding bifurcations. Furthermore, the Lyapunov exponent analysis provided a deeper understanding of the system's chaotic dynamics and the impact of control strategies on stabilizing specific dynamic behaviors.

Z. Huang's[32] study revealed intriguing insights into the dynamic behavior of the shape memory alloy supporter. Through numerical simulations, the researchers generated bifurcation diagrams that showcased the system's responses under different conditions of dissipation, temperature, and frequency parameters. Furthermore, the estimation of Lyapunov exponents provided a deeper understanding of the system's sensitivity to initial conditions. These discoveries not only enriched the understanding of the system's behavior but also demonstrated the effectiveness of the employed numerical methods in capturing and analyzing bifurcation and chaotic phenomena. However, the exitation considered in this study is a periodic signal which is nonrealistic.

The research by M. Varadharajan et al.[7] provided significant insights into the complex dynamics of the quasi-periodically excited three-leg supporter with shape memory alloy. Through the bifurcation analysis, the researchers identified regions of bistability in the system, which can have implications for controllability in mechanical systems. Furthermore, the estimation of Lyapunov exponents using Wolf's algorithm provided crucial insights into the system's behavior. Overall, these investigations offered a comprehensive understanding of the system's dynamics, showcasing bistability behavior and chaotic attractors. However, the exitation used in the above study is a quasi periodic with two terms. This does not show the complex exitation phenomenon that could happen of tripod supporter with three legs.

2.5. Nonlinear Control

2.5 Nonlinear Control

The study by De Paula[30] applied the Extended Time-Delayed Feedback Control (ETDFC) method to stabilize unstable periodic orbits (UPOs) within a chaotic attractor in a nonlinear pendulum system. By adjusting control parameters R and K to target negative Lyapunov exponents, the controller successfully stabilized a period-1 UPO for various R values, including the Traditional Delayed Feedback Control (TDFC) case (R = 0). However, for a period-2 UPO, stabilization was unattainable with R = 0, illustrating the distinction between TDFC and ETDFC. These results demonstrate the effectiveness of the ETDFC method in achieving stability for specific UPOs by manipulating control parameters to influence the system's dynamics and Lyapunov exponents.

Liu and Zheng[34] propose an adaptive robust fuzzy controller, designed to stabilize uncertain chaotic systems by approximating nonlinear functions through fuzzy logic. This approach enhances control performance and robustness, validated through simulations on a unified chaotic system.

Additionally, Rajagopal et al.[35] investigate the dynamics of a Fractional Order Phase Converter with Disturbances and Parameter Uncertainties (PCDPU), developing controllers to suppress chaotic oscillations. Their controllers effectively mitigate chaos within finite time, addressing model uncertainties and parameter variations.

Bessa et al.[36] present an adaptive fuzzy sliding mode controller for uncertain underactuated mechanical systems, combining sliding mode control with fuzzy inference to improve set-point regulation and trajectory tracking. Experimental validation on an overhead container crane confirms its effectiveness.

Building on this, Bessa's[37] study focuses on stabilizing unstable periodic orbits of chaotic systems using an adaptive fuzzy sliding mode controller. This method showcases superior performance in stabilizing chaotic systems with uncertain dynamics and unknown dead-zone inputs, validated through numerical simulations.

In the domain of chaotic system synchronization, Chihn et al.[38] employ Adaptive Fuzzy Sliding Mode Control (AFSMC) to synchronize uncertain fractional-order chaotic systems with time delay,

achieving rapid synchronization through meticulous simulations.

Depaula's[39] comparative study categorizes chaos control methods, emphasizing the success of continuous-time methods like time-delayed feedback and Variable Structure Controller. These methods effectively stabilize unstable periodic orbits observed in SMA structures.

Bessa's[6] utilization of a neuro fuzzy sliding mode controller for vibration stabilization in a two-bar truss highlights the adaptability and robustness of adaptive control strategies, crucial for coping with modeling inaccuracies and external disturbances.

In summary, adaptive fuzzy sliding mode controllers emerge as promising solutions for handling uncertainties in complex systems like SMAs. While other controllers offer simplicity, AFSMC stands out for its adaptability and robustness, making it suitable for nonlinear and uncertain systems.

3

Mathematical Model and stability analysis

In this chapter, the mathematical model for a tripod supporter with SMA (Shape Memory Alloy) bars is developed, employing the Falk polynomial constitutive model to characterize the behavior of the SMA material and incorporating Newton's 2nd law. Then, the stability analysis is performed by calculating the equilibrium points and their respective eigen values. The process involves initially presenting the constitutive model that describes the characteristics of the shape memory alloy material. Subsequently, the equation of motion for the entire system is formulated. The system geometry is described using the figure 3.1[7]. The final mathematical model is employed to calculate the equilibrium and eigenvalues.

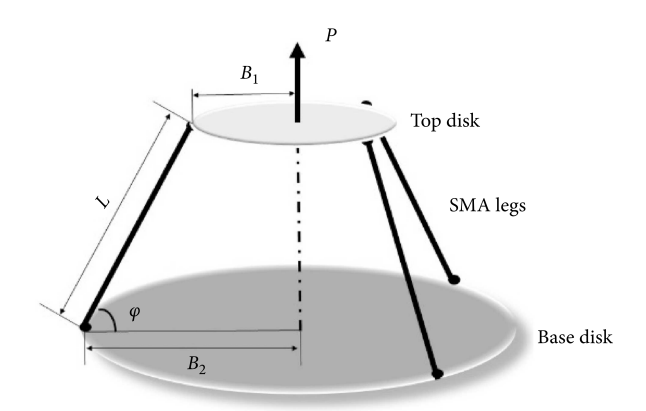


Figure 3.1: System geometry of the SMA supporter

3.1 Mathematical Model

In [32], σ is obtained by describing the shape memory alloy behavior in a polynomial constitutive model[5]. In this paper, the polynomial constitutive model described by Equation (3.1) is used because it requires minimal material parameters and computational power. The polynomial constitutive model:

$$\sigma = a_1(T - T_m)\varepsilon - a_2\varepsilon^3 + a_3\varepsilon^5 \tag{3.1}$$

Where:

- T_m is the temperature below which martensite is stable.
- ε is the strain.
- a_1, a_2, a_3 are the shape memory alloy parameters.
- *T* is the temperature.

The Austenite Temperature is:

$$T_A = T_M + \frac{1}{4} \left(\frac{a_2^2}{a_1 a_3} \right) \tag{3.2}$$

The expression for ε can be obtained using the system geometry: The ε can be expressed using the system geometry:

$$\varepsilon = \frac{L}{L_0} - 1 = \cos\frac{\varphi_0}{\varphi} - 1, \quad L = \sqrt{B^2 + x^2}$$
 (3.3)

Substituting (3.3) into (3.1) gives:

$$\sigma = a_1(T - T_m) \frac{\sqrt{B^2 + x^2}}{L} - 1 - a_2 \left(\frac{\sqrt{B^2 + x^2}}{L} - 1\right)^3 + a_3 \left(\frac{\sqrt{B^2 + x^2}}{L} - 1\right)^5$$
(3.4)

Including (3.4) for σ in the Newtons equation of motion (??) gives us:

$$-3\left(a_{1}(T-T_{m})\frac{\sqrt{B^{2}+x^{2}}}{L}-1-a_{2}\left(\frac{\sqrt{B^{2}+x^{2}}}{L}-1\right)^{3}+a_{3}\left(\frac{\sqrt{B^{2}+x^{2}}}{L}-1\right)^{5}\right)(A)\sin(\varphi)+P=\frac{md^{2}x}{dt^{2}}$$
(3.5)

$$m\frac{d^2X}{dt^2} + c\frac{dX}{dt} + 3A\frac{X}{L_0}\left\{a1(T - T_M)\left(\frac{\sqrt{B^2 + X^2}}{L_0}\right) - a_2\left(\frac{\sqrt{B^2 + X^2}}{L_0}\right)^3 + a_3\left(\frac{\sqrt{B^2 + X^2}}{L_0}\right)^5 = P \quad (3.6)$$

The dimensionless equation becomes:

$$\dot{x} = y
\dot{y} = \gamma(\sin(\Omega_1 \tau) + \sin(\Omega_2 \tau) + \sin(\Omega_3 \tau)) - \xi y
+ x [-((\theta - 1) - 3\alpha_2 + 5\alpha_3)
+ ((\theta - 1) - \alpha_2 + \alpha_3) (x^2 + b^2)^{-\frac{1}{2}}
- (3\alpha_2 - 10\alpha_3) (x^2 + b^2)^{\frac{1}{2}}
+ (\alpha_2 - 10\alpha_3) (x^2 + b^2)
+ 5\alpha_3 (x^2 + b^2)^{\frac{3}{2}} - \alpha_3 (x^2 + b^2)^2]$$
(3.7)

where:

$$w_0^2 = \frac{3Aa_1T_M}{mL_0}, \quad \gamma = \frac{P_0}{mL_0w_0^2}, \quad \xi = \frac{c}{mw_0}, \quad \alpha_2 = \frac{a_2}{a_1T_M}, \quad \alpha_3 = \frac{a_3}{a_1T_M},$$
 $\Omega = \frac{w}{w_0}, \qquad b = \frac{B}{L_0}, \qquad \theta_A = \frac{T_A}{T_M}, \qquad x = \frac{X}{L_0}, \qquad \theta = \frac{T}{T_M}, \qquad \tau = w_0t$

The Simulink model of tripod supporter with SMA bars could be formulated according to the mathe-

matical model developed. The blocks required to form the model are listed as follows;

- State space block: There are two state blocks to represent the state variables of x and y.
- Sine wave block: There are three sine wave blocks to represent the quasi-periodic excitation with three terms.
- Gain blocks: These are blocks that multiply signals by constants like γ , α_2 , α_3 .
- Sum Blocks: These blocks combine the outputs of gain blocks, sine wave blocks, and power blocks.
- Power Blocks: These blocks raise specific terms to the powers of 1/2, 3/2, and 2 as required by the equation.
- Sqare Block: This block calculates the square root of $x^2 + b^2$.

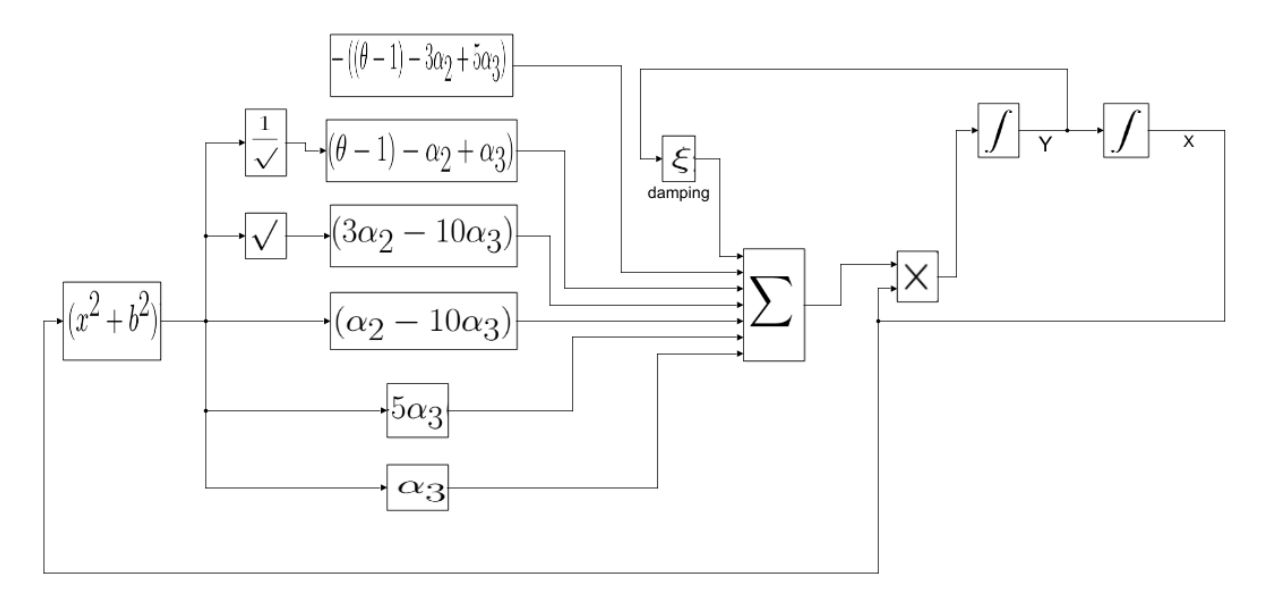


Figure 3.2: System simulink Model

3.2 Stability analysis

The stability of a system could be determined through the process of finding equilibrium points and their respective eigenvalues. Equilibrium point of a set of ordinary differential equation is a solution that does not change with time. It is a point in the state space at which the dynamical system will stay if it starts from that point. It could be found by solving the general equaiton (3.8).

$$\dot{X} = f(x) = 0 \tag{3.8}$$

For the tripod supporter, the equilibrium points are calculated considering the unforced system from equation. The forcing term $\gamma \sin(\Omega_1 \tau) + \sin(\Omega_2 \tau) + \sin(\Omega_3 \tau)$ is discarded from the equation and it is equated to zero as shown in Equation(3.9).

$$0 = y$$

$$0 = \gamma \sin(\Omega_1 \tau) + \sin(\Omega_2 \tau) + \sin(\Omega_3 \tau) - \xi y$$

$$+ x \left[-((\theta - 1) - 3\alpha_2 + 5\alpha_3) + ((\theta - 1) - \alpha_2 + \alpha_3) (x^2 + b^2)^{-\frac{1}{2}} \right]$$

$$- (3\alpha_2 - 10\alpha_3) (x^2 + b^2)^{\frac{1}{2}}$$

$$+ (\alpha_2 - 10\alpha_3) (x^2 + b^2)$$

$$+ 5\alpha_3 (x^2 + b^2)^{\frac{3}{2}} - \alpha_3 (x^2 + b^2)^2$$

$$(3.9)$$

The eigenvalues are determined by finding the jacobian matrix of the system.

The Jacobian matrix for a general system of n first-order differential equations is defined as shown in 3.10:

$$J = \begin{bmatrix} \frac{\partial f_1}{\partial x_1} & \frac{\partial f_1}{\partial x_2} & \cdots & \frac{\partial f_1}{\partial x_n} \\ \frac{\partial f_2}{\partial x_1} & \frac{\partial f_2}{\partial x_2} & \cdots & \frac{\partial f_2}{\partial x_n} \\ \vdots & \vdots & \ddots & \vdots \\ \frac{\partial f_n}{\partial x_1} & \frac{\partial f_n}{\partial x_2} & \cdots & \frac{\partial f_n}{\partial x_n} \end{bmatrix}$$

$$(3.10)$$

where $f_i(x_1, x_2, ..., x_n)$ are the *n* functions describing the system of differential equations, and $x_1, x_2, ..., x_n$ are the variables of the system.

To find the Jacobian matrix for the tripod supporter with SMA system of differential equations, it is done the computing of the partial derivatives of each equation with respect to each variable according to(3.10)

The Jacobian matrix J is given by as shown in 3.11:

$$J = \begin{bmatrix} \frac{\partial \dot{x}}{\partial x} & \frac{\partial \dot{x}}{\partial y} \\ \frac{\partial \dot{y}}{\partial x} & \frac{\partial \dot{y}}{\partial y} \end{bmatrix}$$
(3.11)

where

$$\begin{split} \frac{\partial \dot{x}}{\partial x} &= 0 \\ \frac{\partial \dot{x}}{\partial y} &= 1 \\ \frac{\partial \dot{y}}{\partial x} &= \left[-\left((\theta - 1) - 3\alpha_2 + 5\alpha_3 \right) + \left((\theta - 1) - \alpha_2 + \alpha_3 \right) (x^2 + b^2)^{-\frac{1}{2}} \right. \\ &\left. - \left(3\alpha_2 - 10\alpha_3 \right) (x^2 + b^2)^{\frac{1}{2}} + \left(\alpha_2 - 10\alpha_3 \right) (x^2 + b^2) + 5\alpha_3 (x^2 + b^2)^{\frac{3}{2}} - \alpha_3 (x^2 + b^2)^2 \right] \\ \frac{\partial \dot{y}}{\partial y} &= -\xi \end{split}$$

Then, the Jacobian matrix J for the tripod supporter according (3.11) is given by (3.12):

$$J = \begin{bmatrix} 0 & 1 \\ A & -\xi \end{bmatrix} \tag{3.12}$$

where A

$$A = -((\theta - 1) - 3\alpha_2 + 5\alpha_3) + ((\theta - 1) - \alpha_2 + \alpha_3)(x^2 + b^2)^{-\frac{1}{2}}$$

$$-(3\alpha_2 - 10\alpha_3)(x^2 + b^2)^{\frac{1}{2}}$$

$$+(\alpha_2 - 10\alpha_3)(x^2 + b^2) + 5\alpha_3(x^2 + b^2)^{\frac{3}{2}} - \alpha_3(x^2 + b^2)^2$$

The characteristic equation of a matrix J is given by as shown in (3.13)

$$|J - \lambda I| = 0 \tag{3.13}$$

where I is the identity matrix. Substituting Equation (3.13) into the characteristic Equation (3.14), gives (3.14):

$$\begin{bmatrix} -\lambda & 1 \\ A & -\xi - \lambda \end{bmatrix} = 0 \tag{3.14}$$

Expanding the determinant, we have (3.15):

$$(-\lambda) \cdot (-\xi - \lambda) - (A \cdot 1) = 0 \tag{3.15}$$

Simplifying (3.15) gives Equation (3.16):

$$\lambda^2 + \xi \lambda + A = 0 \tag{3.16}$$

This is the characteristic equation for the tripod supporter with SMA system. The above way of stability analysis could be treated analytically or numerically employing matlab code. The matlab code required to find the equilibrium points and eigen values is provided in the Appendix A.

4

Non-linear analysis and AFSMC design

4.1 Dynamical analysis

4.1.1 Phase Portrait

A phase portrait is a diagram that illustrates all qualitatively different trajectories of a system. In a phase portrait, a point is imagined to move along the real line according to the local velocity f(x). When f(x) > 0, the point moves in the right direction, and when f(x) < 0, the point moves in the left direction [40].

The appearance of a phase portrait is determined by the fixed points, also known as equilibrium

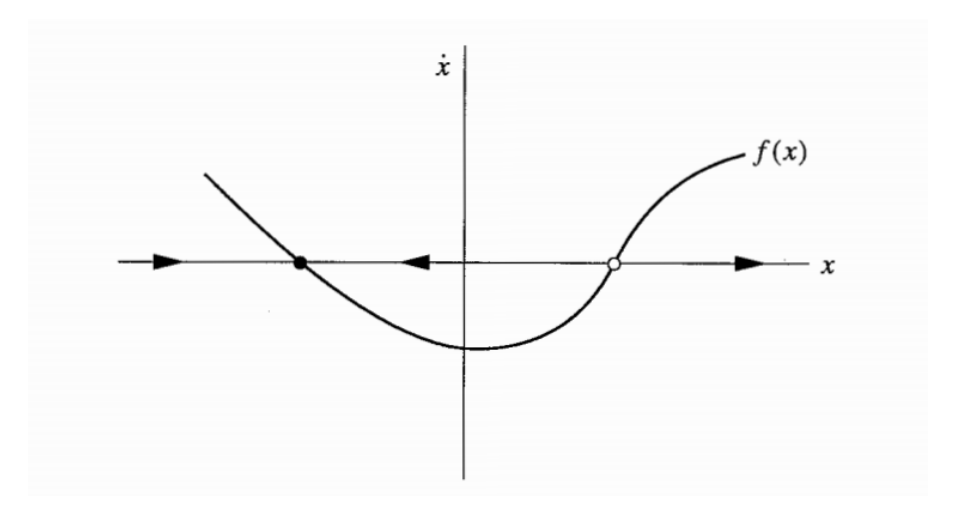


Figure 4.1: Phase Space

points. Stable fixed points (where small perturbations will damp out over time) are represented in a phase portrait by solid black dots, while unstable fixed points (where small perturbations will grow) are represented by open dots.

Phase portraits can be generated using various methods, including computer simulation, analytical methods, and the method of isoclines. Numerical computer simulation is widely used due to its simplicity. There is a MATLAB function program called pplane8 that can generate phase portraits, and it is also possible to generate them using the Simulink XY scope.

Analytical methods are limited to generating phase portraits for only simple differential equations and piecewise linear systems. The method of isoclines can handle all nonlinearities; however, it is computationally challenging.

The phase portrait of the tripod supporter with a shape memory alloy supporter is simulated by numerically integrating the system dynamics and correlating the velocity and displacement in the x-y graph. The Simulink XY plot is used to display the phase portrait of the tripod supporter with the S-MA system. The Simulink model of the system used to simulate the phase portrait is shown in Figure 4.2.

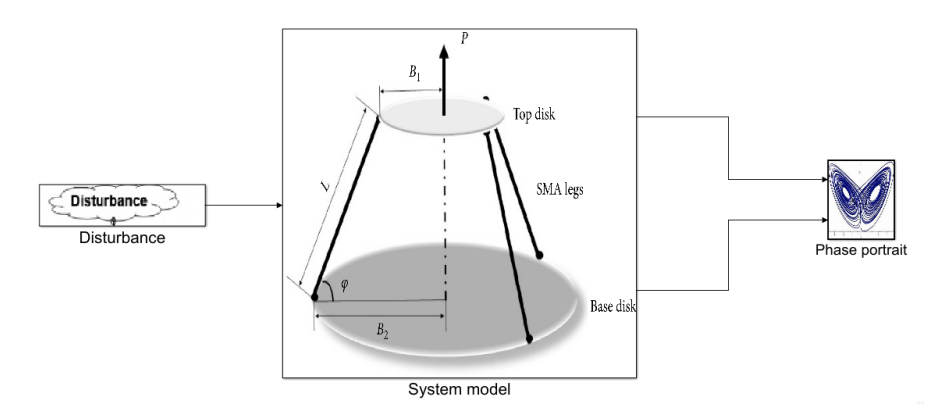


Figure 4.2: Simulink Model for Phase Portrait Simulation

4.1.2 Bifurcation

The approach utilized to generate the bifurcation diagram involves identifying the peaks of the xcoordinate as γ or ξ increases gradually. This process effectively pinpoints the range where the system
exhibits bistability. The methodology could be implemented by employing a MATLAB function
detailed in AppendixB, which generates both forward and backward continuation simulations. The
flowchart depicting the sequential steps of this MATLAB function is illustrated in Figure (4.3).

To elaborate, the method iteratively explores the parameter space, incrementally adjusting γ or ξ while monitoring the resulting behavior of the system. At each step the local maxima of the *x*-coordinate are identified. These maxima incomparison with the reverse continuation maxima signify the regions of bistability where the system can exhibit multiple stable states. By systematically traversing the parameter space in this manner, a comprehensive understanding of the system's behavior and bistable regions is attained.

4.1.3 Lyapunov Exponents

The calculation of Lyapunov Exponents (LEs) is a fundamental technique in the analysis of dynamical systems to understand their stability and chaotic behavior. The Lyapunov Exponents quantify the exponential rates of divergence or convergence of nearby trajectories in the system's phase space.

Lyapunov exponent describes the system trajectories convergence or sensitivity to initial condition. If there is one positive Lyapunov exponent, the system is called chaotic system. This means for a small

Bifurcation Analysis Flowchart Clear workspace -Define global variables -Initialize parameters -Define simulation step Set up -Set initial conditions -Set parameter range of interest -Presave a matrix of NaNs : Set ODE options -Discard transient -Find local maxima Simulate the system -Store results parameter range Set initial conditions for second range Presave a matrix of NaNs -Discard transient Simulate the system -Find local maxima -Store results second parameter range Plot the result

Figure 4.3: Flowchart for bifurcation diagram simulation

variation of initial condition the system trajectory diverges. If all Lyapunov exponents are negative then the system does not diverge for a small variation of initial condition.

The calculation of Lyapunov Exponents employing the system mathematical model is complex and it takes a lot of time. However, using matlab buildin function the largeset lyapunov exponent of a system could be obtained by using input the systems time series trajectories. The builtin function can be writen as LLE= lyapunovexponent(x, f_s) where x is the systems timeseries trajectory and f_s is the sampling time used to obtain the trajectory. The Lyapunov Exponents are then examined to determine the stability and chaotic behavior of the system.

4.2 Controller Design

4.2.1 Adaptive Fuzzy Sliding Mode Control

Sliding mode control is a method that transforms system dynamics into a new stable compensated form within finite time, damping these dynamics asymptotically. The following section outlines the methodology utilized for designing the sliding mode controller. Upon incorporating the control variable into the ordinary differential equation (ODE), it takes the form:

$$\frac{dx}{dt} = y, \quad \frac{dy}{dt} = f + d + u \tag{4.1}$$

where:

- *u* represents the control action,
- d denotes the external disturbance given by $\gamma(\sin(\omega_1) + \sin(\omega_2) + \sin(\omega_3))$,
- The function f is defined as:

$$f = -\xi y + x \left[-\left((\theta - 1) - 3\alpha_2 + 5\alpha_3 \right) + \left((\theta - 1) - \alpha_2 + \alpha_3 \right) (x^2 + b^2)^{-\frac{1}{2}} - \left(3\alpha_2 - 10\alpha_3 \right) (x^2 + b^2)^{\frac{1}{2}} + \left(\alpha_2 - 10\alpha_3 \right) (x^2 + b^2) + 5\alpha_3 (x^2 + b^2)^{\frac{3}{2}} - \alpha_3 (x^2 + b^2)^2 \right]$$

Several assumptions are made:

- 1. The state vector *x* is accessible.
- 2. The function f is unknown but bounded by a known function of x.
- 3. The disturbance d is unknown but bounded by $|d| \le D$.

The compensated dynamics is represented by:

$$\sigma = y + \lambda x \tag{4.2}$$

Resulting in the equivalent control:

$$u = -\hat{f} - d - \lambda y - k \operatorname{sat}\left(\frac{s}{\phi}\right) \tag{4.3}$$

Where $sat(s/\phi)$ is introduced to ensure system robustness, with ϕ being a strictly positive constant. The gain k is determined as stated in Equation (4.4):

$$k \ge \eta + F + D + |\hat{d}| \tag{4.4}$$

Where η is a strictly positive constant associated with the time required to attain the sliding surface.

The adaptive fuzzy approach is employed to approximate the disturbance d effectively. Fuzzy systems serve as universal approximators, capable of approximating any function with arbitrary accuracy. The zero-order Takagi-Sugeno-Kang (TSK) fuzzy inference system is adopted, with rules defined in the following linguistic form.

If s is S_r , then $d_r = D_r$; r = 1, 2, ..., N, where S_r are fuzzy sets with appropriately chosen membership functions, and D_r represents the output value of each of the N fuzzy rules.

The estimated disturbance $\hat{d}(s)$ is computed using a weighted average of the outputs \hat{d}_r , determined by the weights w_r . These weights are based on the firing strength of each rule. To improve the estimate accuracy, the vector of adjustable parameters **D** is updated using an adaptation law, taking into account the system state s and the firing strengths as stated in Equation (4.5):

$$\dot{\hat{D}} = \vartheta \Psi(s) \tag{4.5}$$

where ϑ is a positive constant of the adaptation rate. The Simulink models depicting the tripod system with the AFSMC and the sliding mode controller are presented in Figures 4.4 and 4.5, respectively.

4.2.2 Controller Performance Assessment Criteria

The performance of a controller is crucial for evaluating its effectiveness in maintaining the system within desired parameters. Various criteria are employed to assess this performance, capturing different aspects such as error magnitude, time response, and stability characteristics.

4.2.2.1 Integral Absolute Error (IAE)

Integral Absolute Error (IAE) is a commonly used criterion for evaluating controller performance. It quantifies the cumulative absolute deviation of the system output from the desired setpoint over time. Mathematically, IAE is defined as:

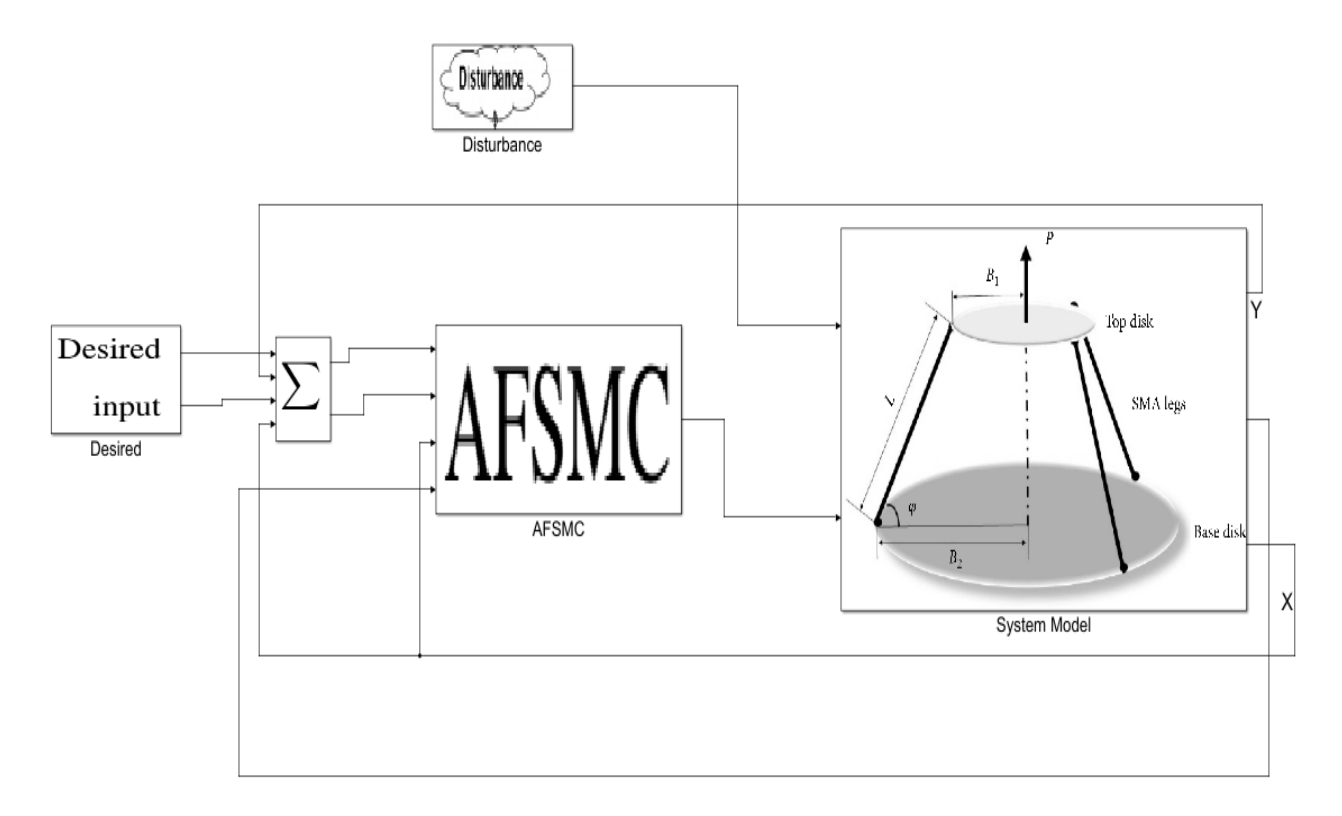


Figure 4.4: Tripod system with the AFSMC

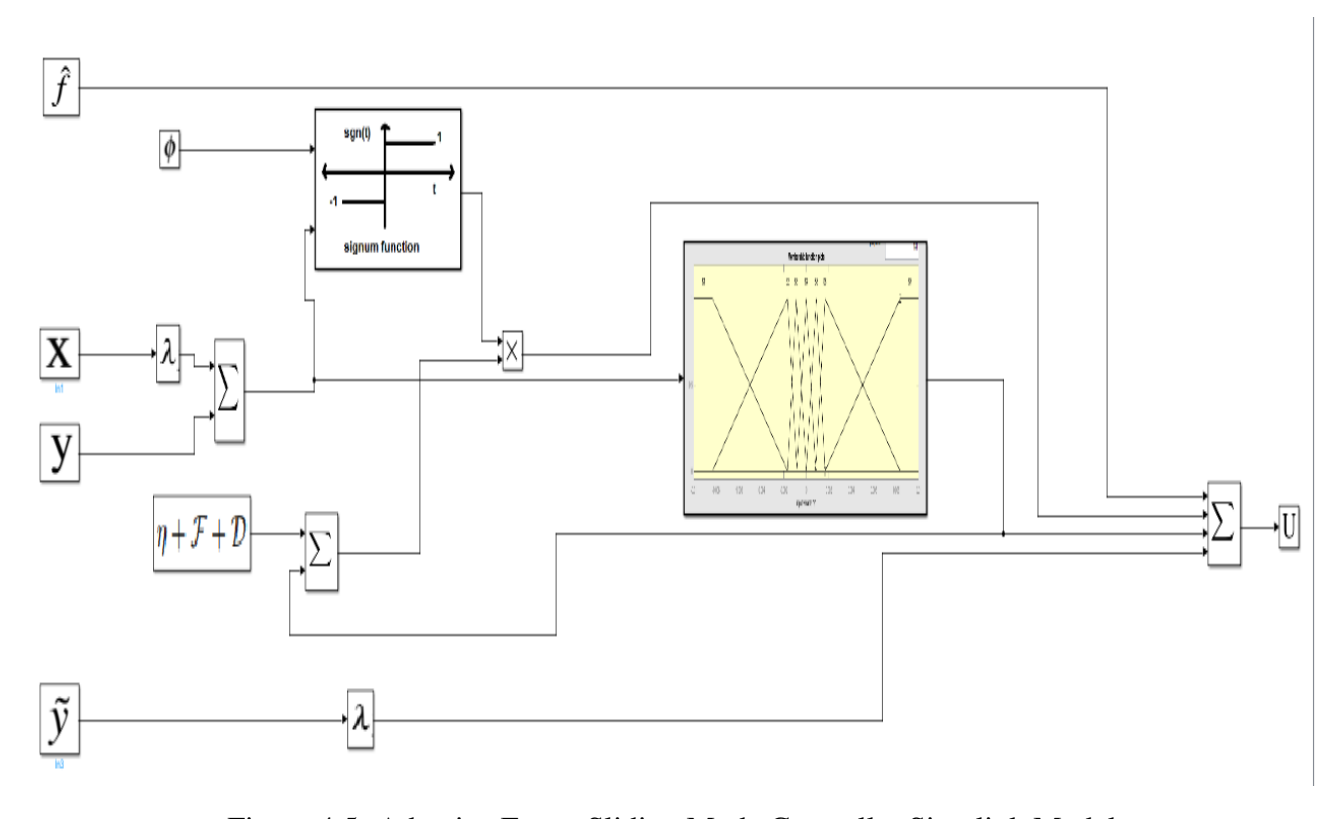


Figure 4.5: Adaptive Fuzzy Sliding Mode Controller Simulink Model

$$IAE = \int_0^\infty |y_{dp}(t) - y_a(t)| dt \tag{4.6}$$

Where:

- $y_{dp}(t)$ is the desired setpoint,
- $y_a(t)$ is the actual system output.

The integral in Equation 4.6 sums up the absolute differences between the desired setpoint and the actual output over the entire time horizon.

4.2.2.2 Integral Time Absolute Error (ITAE)

Integral Time Absolute Error (ITAE) is another performance criterion that considers both the error magnitude and the time it takes to reach a steady state. It is defined as the integral of the absolute error weighted by time:

$$ITAE = \int_0^\infty t |y_{dp}(t) - y_a(t)| dt$$
(4.7)

Similar to IAE, ITAE penalizes larger errors more severely, with an additional emphasis on minimizing the settling time.

4.2.2.3 Integral Square Error (ISE)

Integral Square Error (ISE) focuses on minimizing the squared error between the desired setpoint and the actual output over time. It is given by:

$$ISE = \int_0^\infty |(y_{dp}(t) - y_a(t))^2| dt$$
 (4.8)

ISE provides a measure of the overall deviation of the system response from the desired trajectory, with larger errors contributing significantly to the total score.

4.2.2.4 Undershoot and Overshoot

Undershoot and overshoot are crucial performance metrics, especially in systems where rapid response and stability are paramount.

Undershoot refers to the phenomenon where the system's output initially falls below the desired setpoint before reaching steady-state. It is quantified as the maximum negative deviation from the setpoint.

Overshoot, on the other hand, occurs when the system's output exceeds the desired setpoint before stabilizing. It is measured as the maximum positive deviation from the setpoint.

4.2.2.5 Fall Time

Fall time measures the time taken by the system's response to transition from a specified percentage (e.g., 90

These additional performance metrics provide comprehensive insights into the behavior and effectiveness of control systems, aiding in the selection and tuning of controllers for optimal performance.

5

Result and Discussion1

5.1 Introduction

This chapter presents the outcomes of numerical simulations investigating the nonlinear dynamics of a tripod supporter with shape memory alloy (SMA) and its integration with Adaptive Fuzzy Sliding Mode Control (AFSMC). Initially, the equilibrium points and their stability are delineated. Subsequently, the analysis results aim to shed light on the system's behavior during the martensite, austenite, and transition phases. The chapter is structured accordingly, focusing on each phase. Within each phase, simulations encompass phase portraits, bifurcations, and Lyapunov exponents assessments under quasi-periodic excitation with three terms. The influence of the AFSMC on system behavior over time will be stated through the obtained results. System parameters are adopted from the study con-

ducted by Huang et al. (2008) [32], where $\alpha_2 = 124$, $\alpha_3 = 14505$, b = 0.7071, $\gamma = 0.045$, and the frequencies of the quasi periodic signal are taken $\Omega_1 = 0.5$, $\Omega_2 = ((\sqrt{5} - 1)/2)$, and $\Omega_3 = \Omega_1 + \Omega_2$.

5.2 Equilibrium Points and Their Stability

The equilibrium points for the tripod supporter with SMA, are found to be $E_1 = (0,0)$ and $E_2 = (0,-0.552)$ as depicted in Figure (5.1).

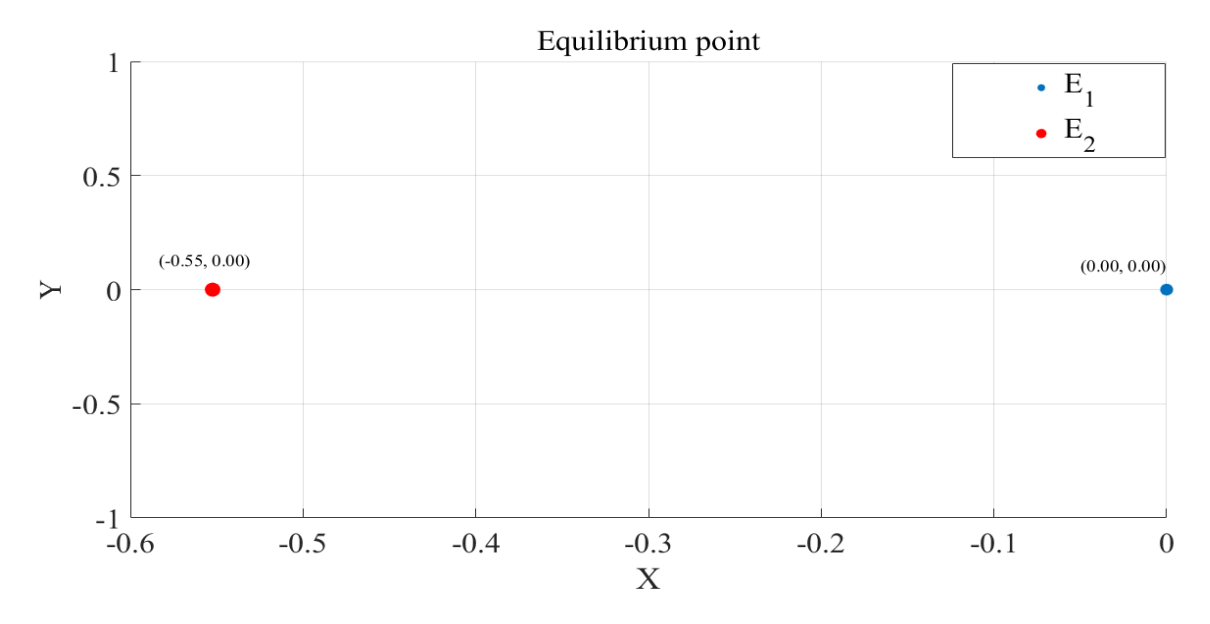


Figure 5.1: Equilibrium Points

These equilibrium points represent stable or unstable configurations of the system where the net forces and torques acting on it are balanced.

Their respective eigenvalues describe the behavior of small perturbations around these equilibrium points. For equilibrium point 1 (E_1), the eigenvalues are $\lambda_1 = 6.25$ and $\lambda_2 = -6.35$. This indicates that equilibrium point 1 is a saddle point, which is unstable. For equilibrium point 2 (E_2), the eigenvalues are $\lambda_1 = -0.05 - 1.2i$ and $\lambda_2 = -0.05 + 1.2i$. This suggests that equilibrium point 2 is a stable spiral.

The eigenvalues are depicted in Figure (5.2).

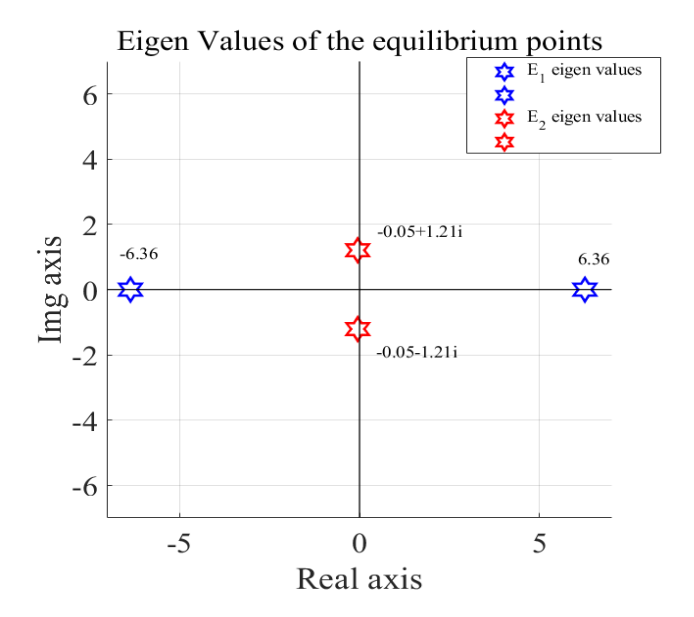


Figure 5.2: Eigenvalues

5.3 Dyanamics in Martensite phase

In this case low temperature ($\theta = 0.69$) martensite phase is considered and the dynamical behaviour during this phase is analysed using phase portrait, bifurcation diagram, and Lyapunov exponent simulation.

To simulate the phase portrait, the model is supplied with parameters $\alpha_2 = 124$, $\alpha_3 = 14505$, b = 0.7071, and the frequencies of the quasi periodic signal are taken as $\gamma = 0.045$, $\Omega_1 = 0.5$, $\Omega_2 = ((\sqrt{5}-1)/2)$, and $\Omega_3 = \Omega_1 + \Omega_2$. Two damping conditions are considered: one with $\xi = 0.1$ and the other with $\xi = 1.5$.

For $\xi = 0.1$, the system exhibits chaotic behavior with a strange attractor.

The phase portrait depicted in Figure (5.3) illustrates the complex behavior of the system under the damping condition $\xi = 0.1$. The presence of a strange attractor indicates chaotic dynamics, where the system's trajectory appears highly sensitive to initial conditions, resulting in seemingly random behavior over time.

For a higher value of the damping coefficient, the system does not exhibit chaotic behavior. Specifically, for $\xi = 1.5$, the system exhibits attracting tori.

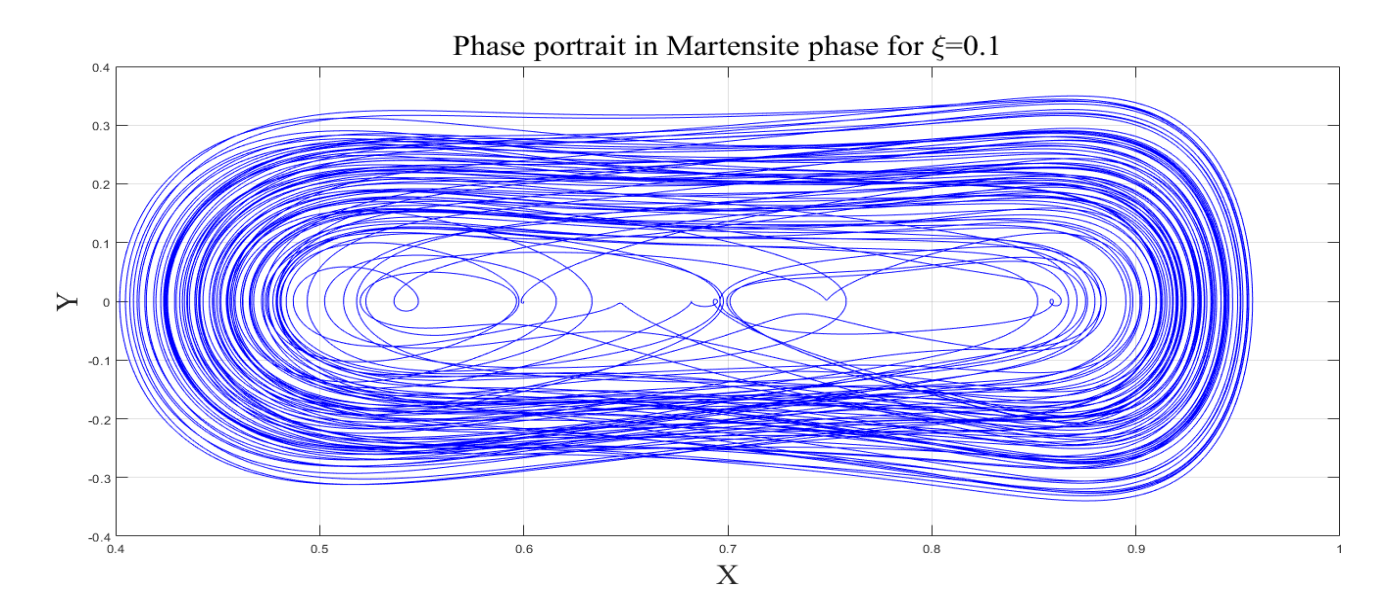


Figure 5.3: Phase portrait for $\xi = 0.1$

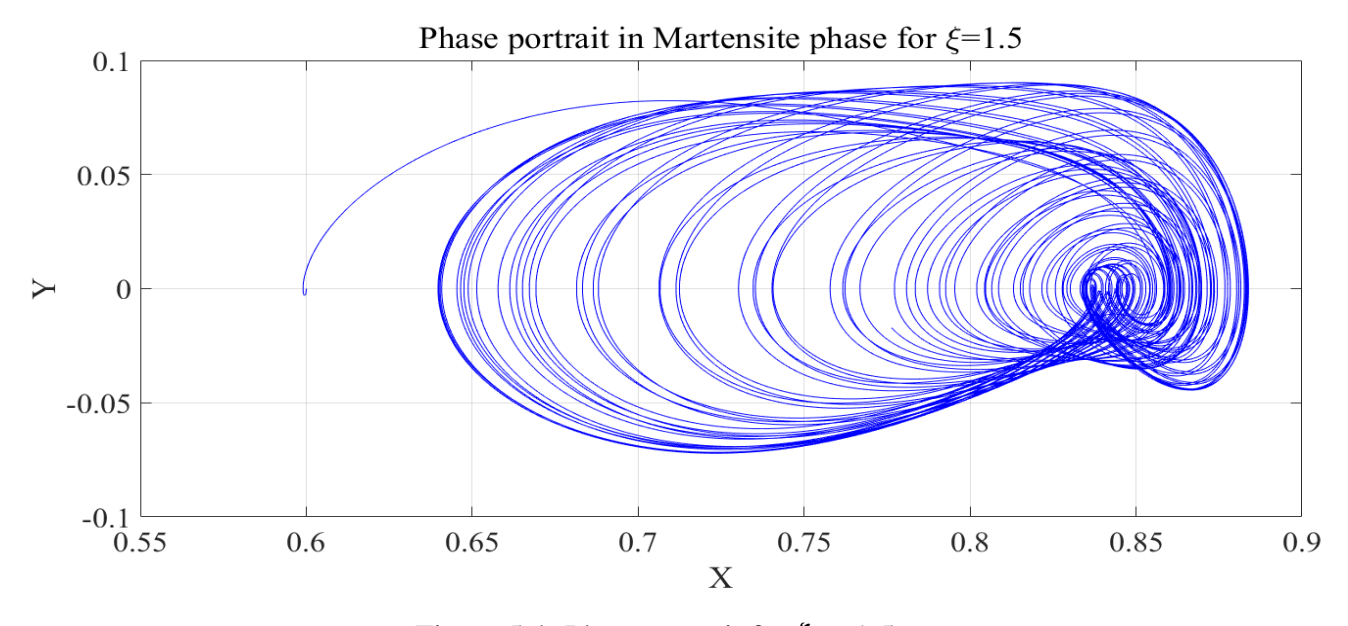


Figure 5.4: Phase portrait for $\xi = 1.5$

Figure (5.4) displays the phase portrait for $\xi = 1.5$. Unlike the chaotic behavior observed for $\xi = 0.1$, the system under this damping condition demonstrates the presence of attracting tori. These tori indicate stable periodic motion, where the system's trajectory converges to specific attractor surfaces rather than exhibiting chaotic dynamics.

These results underscore the significant influence of the damping coefficient ξ on the system's behavior. A low damping coefficient can lead to chaotic dynamics characterized by a strange attractor, while a higher damping coefficient promotes stability and periodic motion, as evidenced by the presence of attracting tori.

The Lyapunov exponent calculated using [41] indicates a positive largest Lyapunov exponent $\lambda = 0.206$ when $\xi = 0.1$, suggesting the existence of chaos. Conversely, for $\xi = 1.5$, both Lyapunov exponents are negative, signifying the absence of chaos. The positive Lyapunov exponent describes the system's sensitivity to the initial condition. The time series for $\xi = 0.1$ and for close initial conditions (0.6,0) and (0.60001,0) illustrate this sensitivity, as depicted in Figure 5.5.

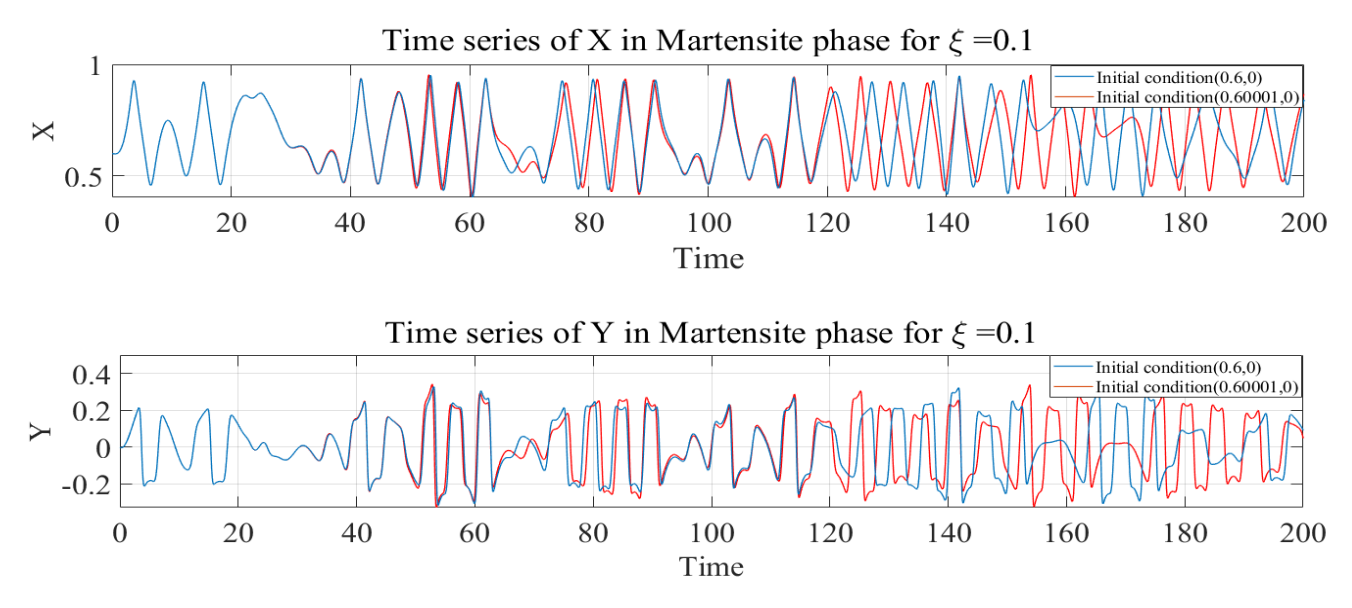


Figure 5.5: Time series for $\xi = 0.1$, showing sensitivity to initial conditions

The negative Lyapunov exponent indicates the convergence of the system for close initial conditions. The time series for $\xi = 1.5$ and for close initial conditions (0.6,0) and (0.60001,0) illustrate this convergence, as shown in Figure 5.6.

Bifurcation diagrams serve as indispensable tools for qualitatively describing the system's behavior,

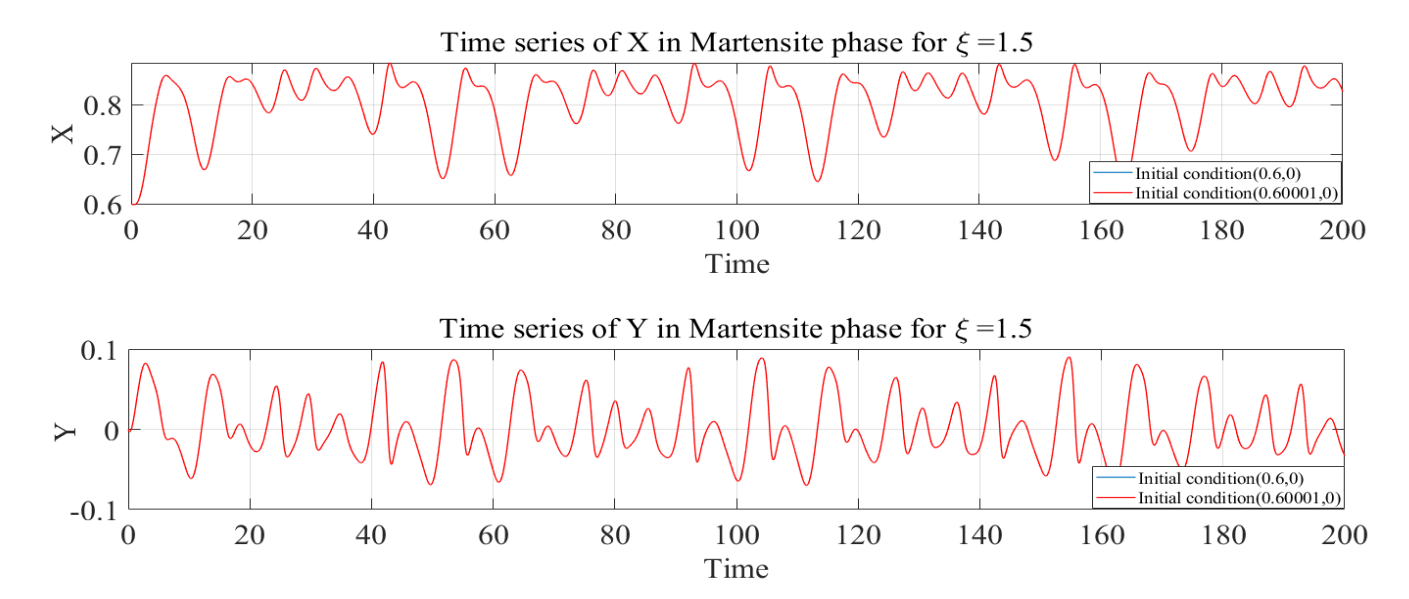


Figure 5.6: Time series for $\xi = 1.5$, demonstrating convergence for close initial conditions

particularly regarding bistability, across a spectrum of parameters, including γ and ξ . This analysis is pivotal for comprehending how the system manifests bistability under diverse parameter configurations. By maintaining other parameters constant, the bifurcation diagram examines the change in behaviour for varying γ through both forward and backward continuation methods, with $\xi=0.1$, thereby unveiling a bistability condition. The coexistence of forward (blue) and backward (red) branches in Figure (5.7) attests to this bistable nature.

Bistability, though occasionally advantageous in specific applications, can introduce complications and adverse effects in others. For instance, it can engender unpredictable behavior and instability within control systems, impeding the attainment of desired performance or the maintenance of system stability over time. Moreover, bistability may increase the complexity of system analysis and design, potentially prolonging development timelines and increasing associated costs.

Furthermore, the assessment of bifurcation diagrams for varying damping parameters also underscores the existence of bistability, as evidenced in Figure (5.8).

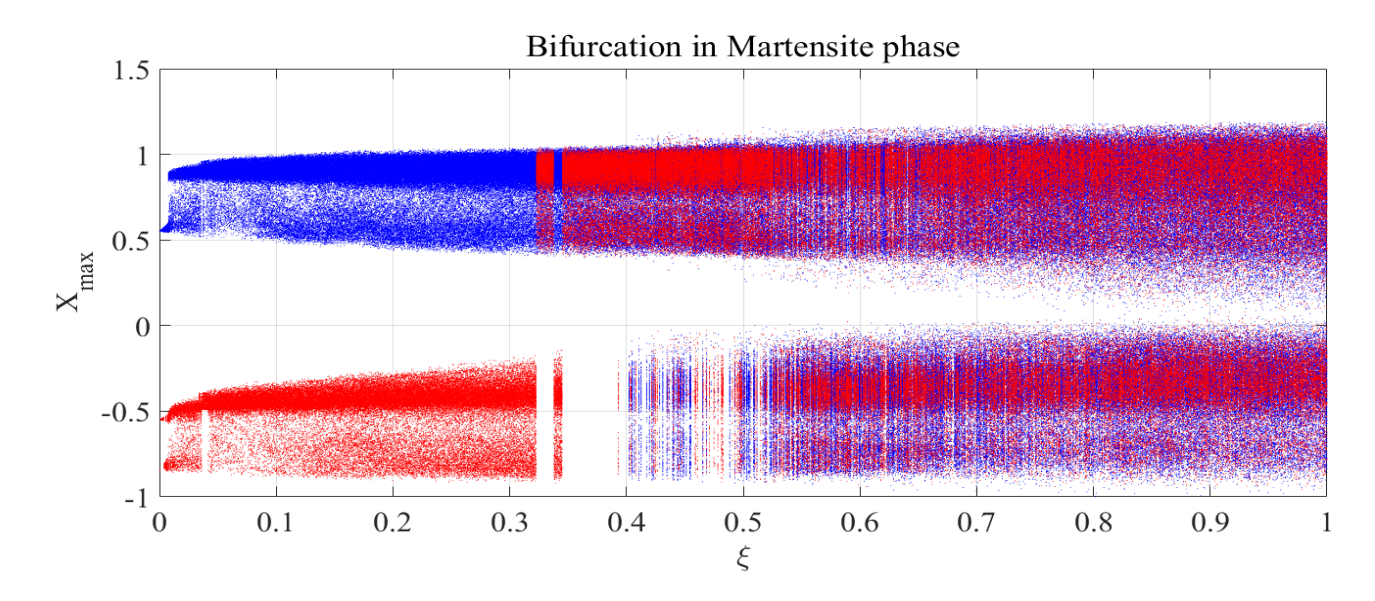


Figure 5.7: Bifurcation diagram for varying γ with $\xi=0.1$

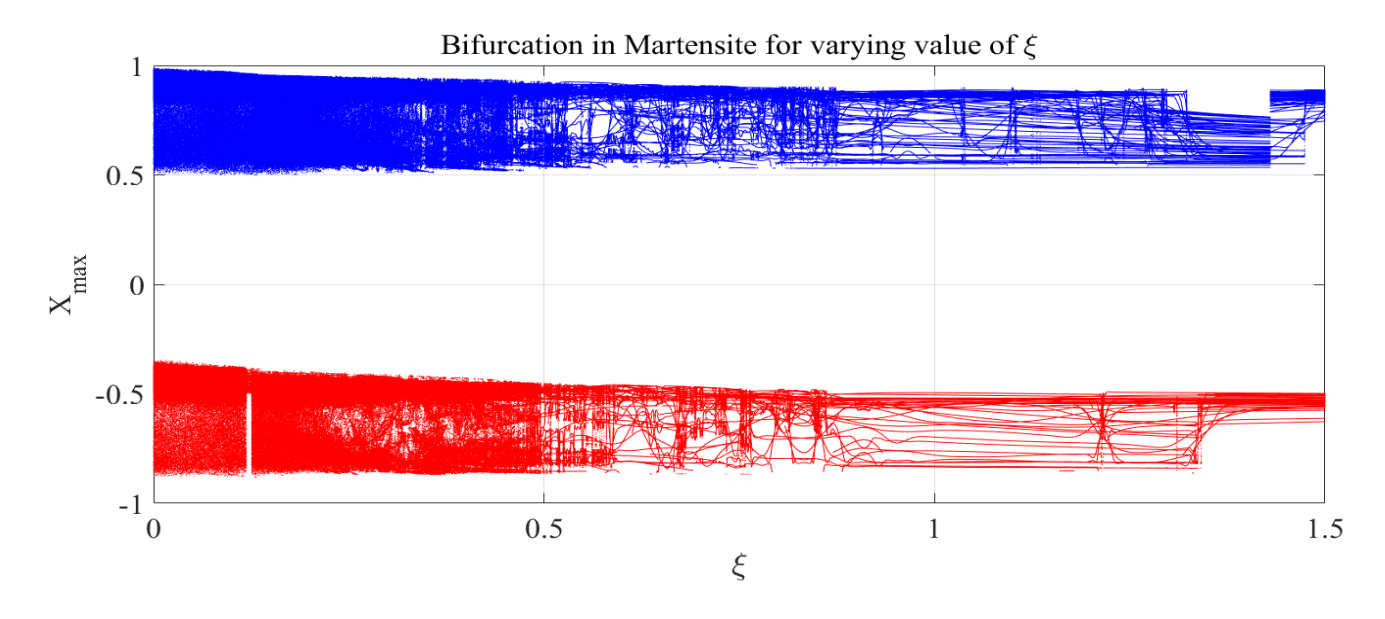


Figure 5.8: Bifurcation diagram for varying ξ

5.4 Dynamics in Transition phase

In this case a temperature where transition from martensite to austenite phase occurs is considered. This phase consists both phases. The temperature coefficient $\theta=1.04$ is in the transition phase. Since small damping coefficient doesn't have much effect on the system dynamics for $\xi=0.1$ the system shows a chaotic attractor. For higher damping coefficient the system have an attracting tori

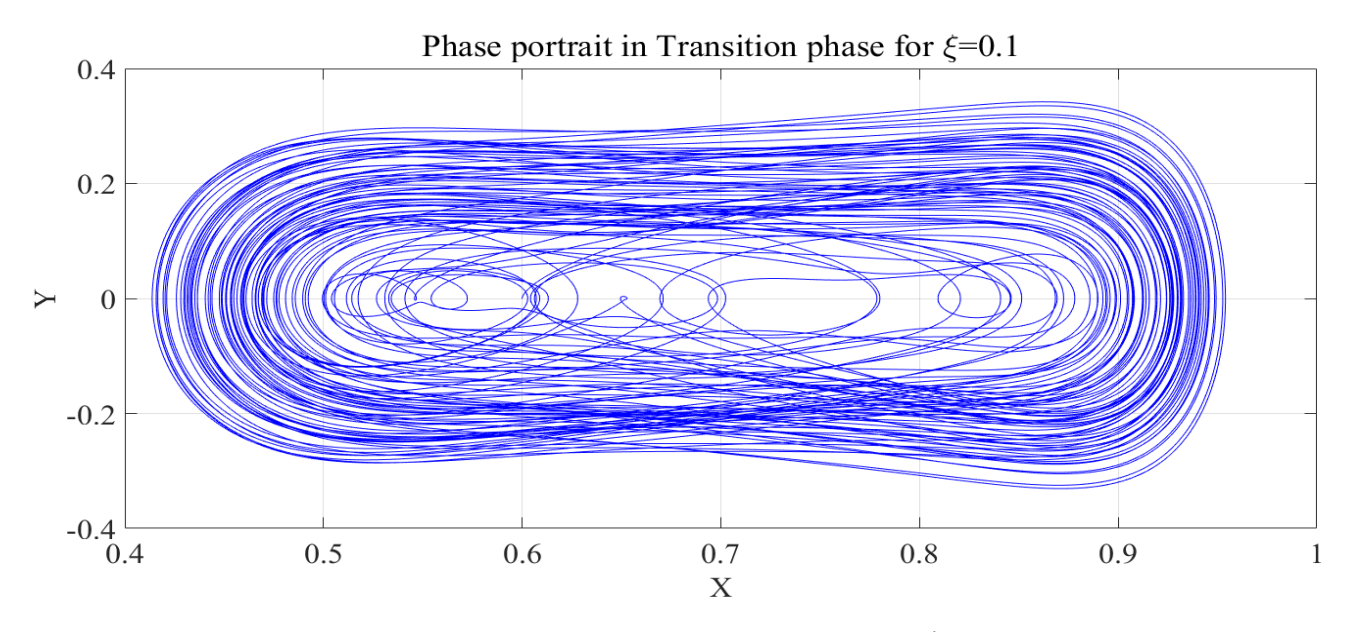


Figure 5.9: Phase portrait in transition phase for $\xi = 0.1$

behaviour. A positive largest Lyapunov exponent $\lambda = 0.18$ when $\xi = 0.1$ for the transition phase,

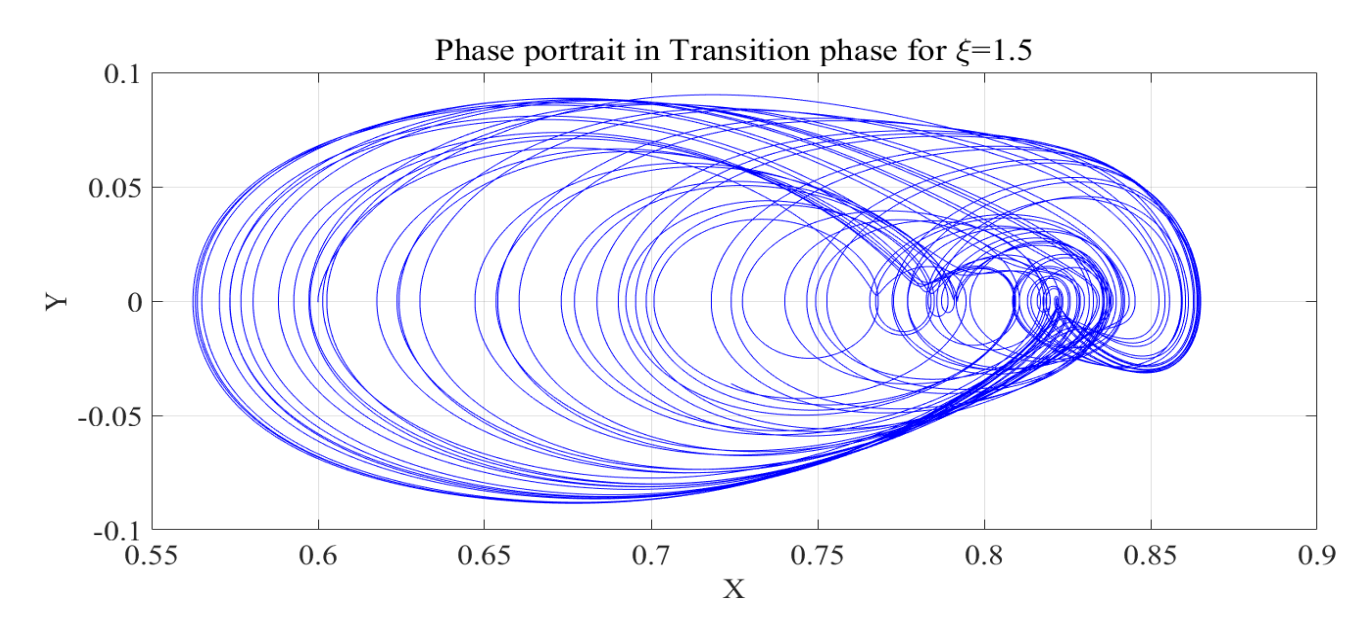


Figure 5.10: Phase portrait in transition phase for $\xi = 1.5$

suggesting the existence of chaos. Conversely, for $\xi=1.5$, both Lyapunov exponents are negative, signifying the absence of chaos. The positive Lyapunov exponent describes the system's sensitivity to the initial condition. The time series for $\xi=0.1$ and for close initial conditions (0.6,0) and (0.60001,0) illustrate this sensitivity, as depicted in Figure(5.11). The trajecotries begin to diverge at the time around 45sec.

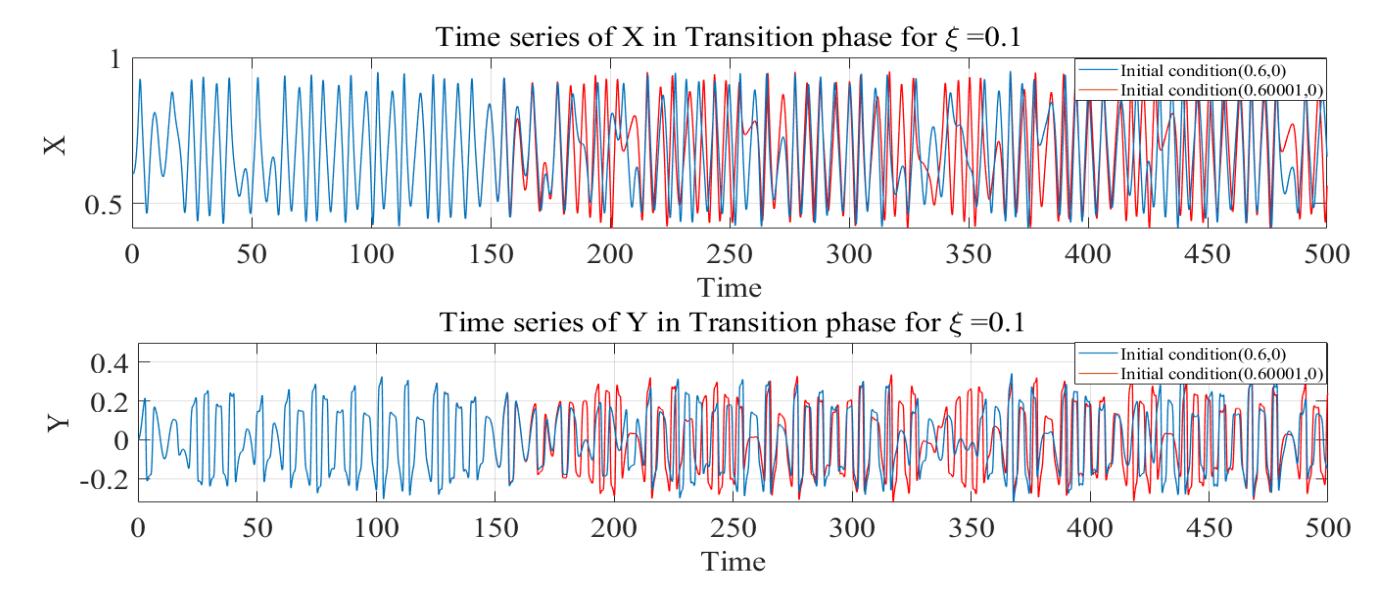


Figure 5.11: Time series for $\xi = 0.1$, showing sensitivity to initial conditions

The negative Lyapunov exponent indicates the convergence of the system for close initial conditions. The time series for $\xi = 1.5$ and for close initial conditions (0.6,0) and (0.60001,0) illustrate this convergence, as shown in Figure (5.12).

The forward and backward continuation bifurcation diagram for varying amount of γ shows bistability in the region from $\gamma = 0$ to 0.0005 as shown in Figure (5.13).

5.5 Dynamics in Austensite Phase

The austenite phase is stable at high temperatures. The phase portrait for small damping coefficients exhibits a chaotic attractor as shown in Figure (5.14). For a higher value of the damping coefficient $\xi = 1.5$, the system exhibits attracting tori as shown in Figure (5.15).

The Lyapunov exponent for $\xi = 0.1$ is a positive number 0.17, which shows the system's chaotic

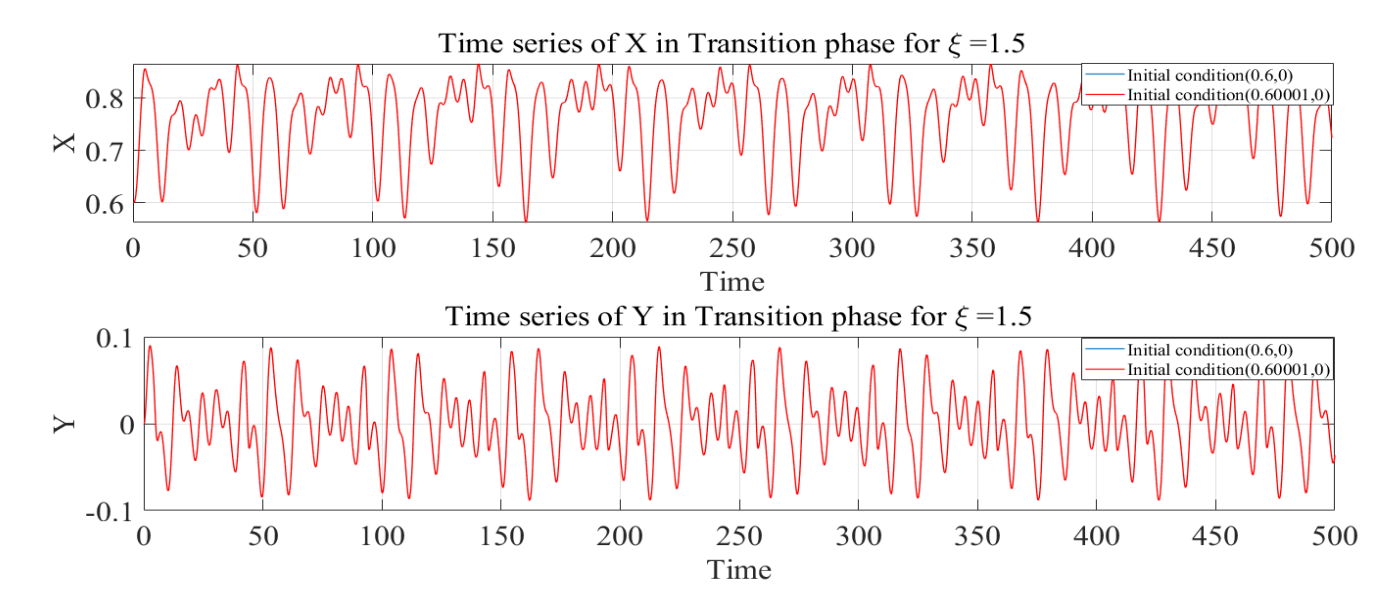


Figure 5.12: Time series for $\xi = 1.51$, showing convergence to initial conditions

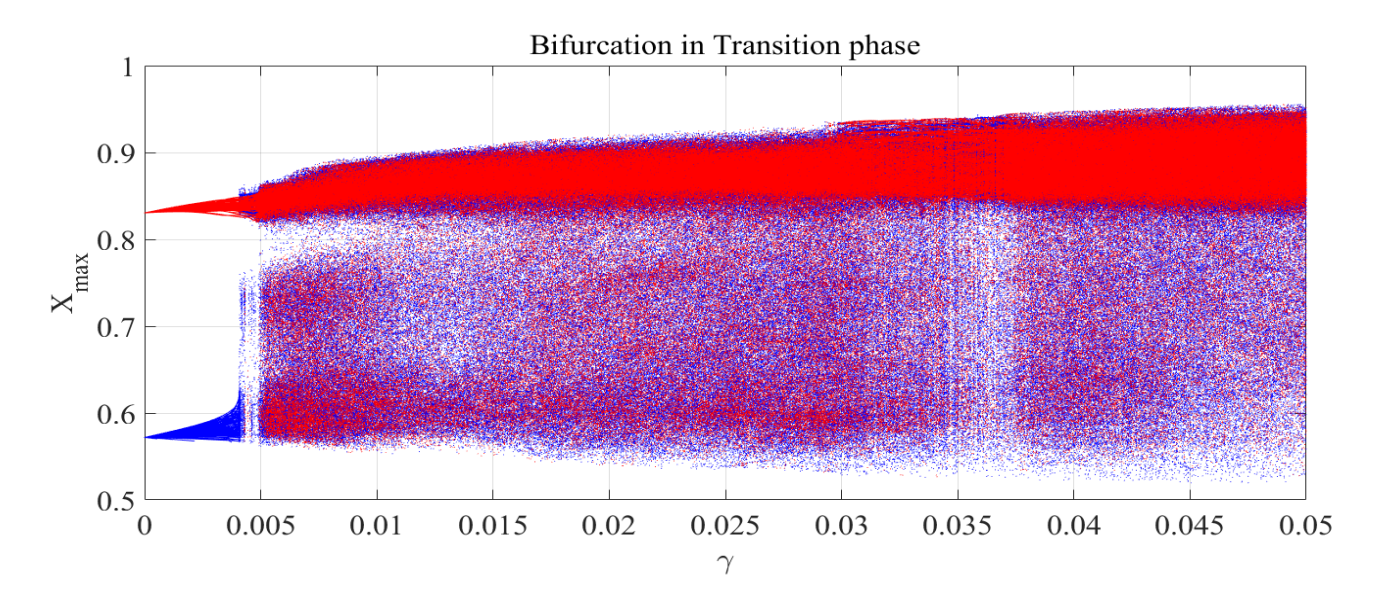


Figure 5.13: Bifurcation in transition phase for $\xi = 0.1$

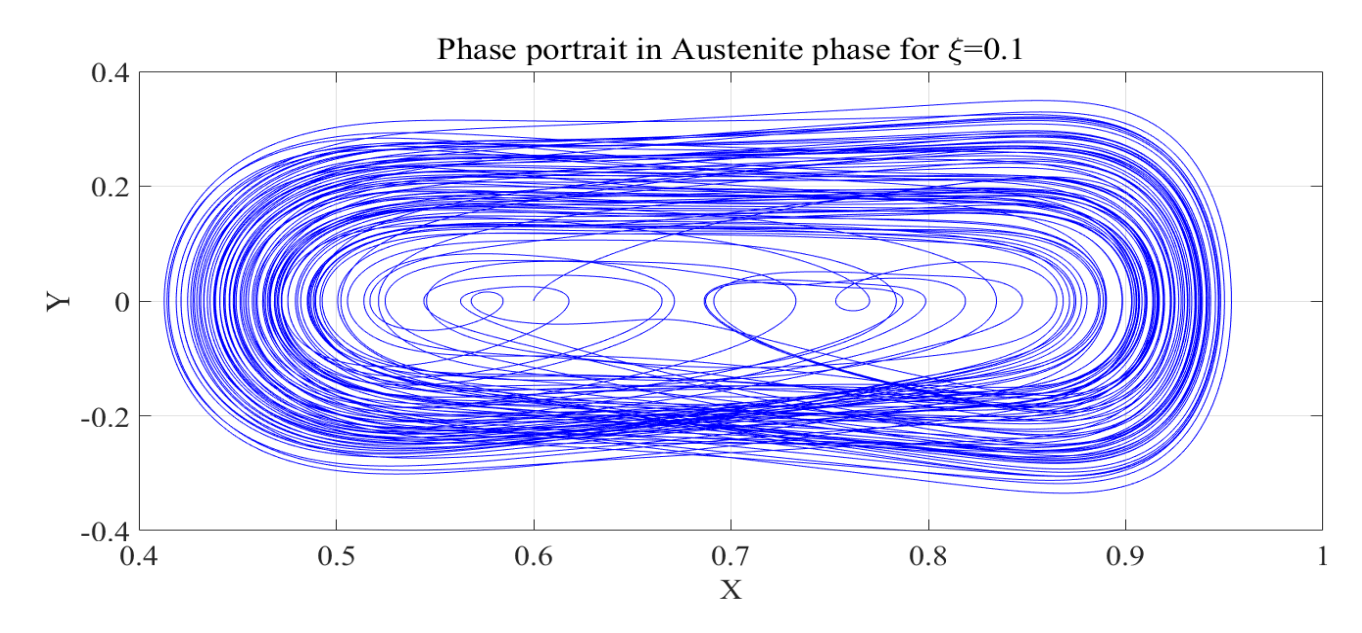


Figure 5.14: Phase portrait in Austenite phase for $\xi=0.1$

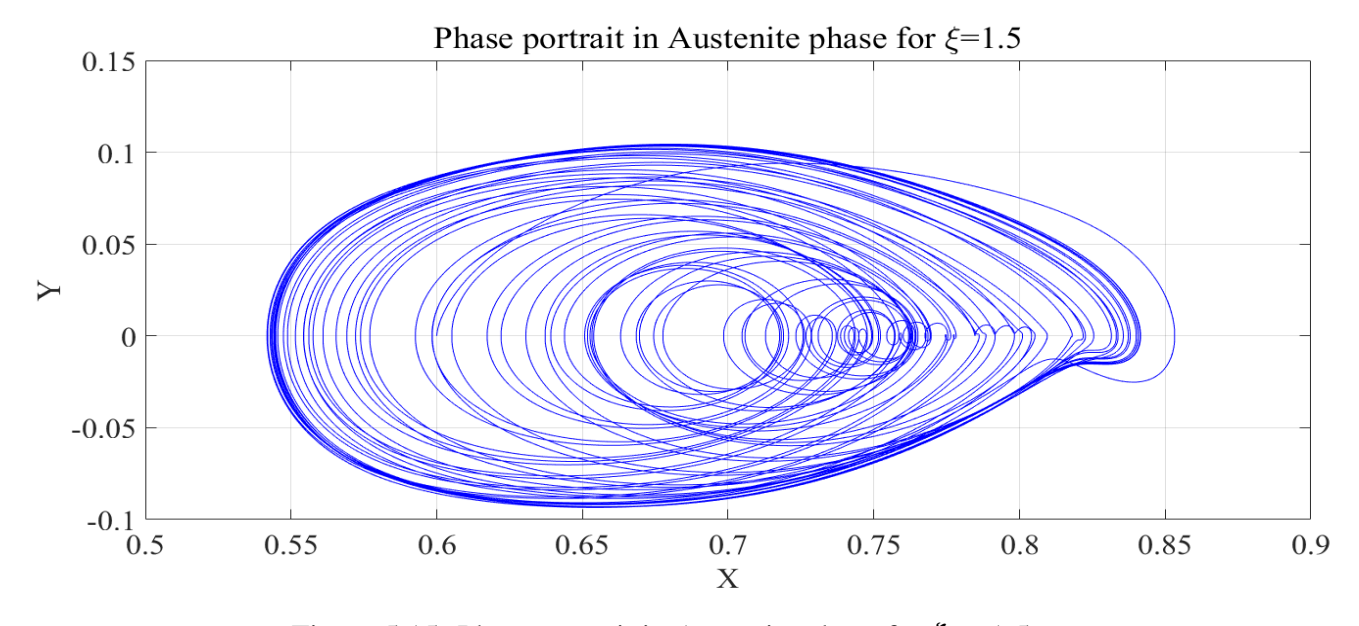


Figure 5.15: Phase portrait in Austenite phase for $\xi=1.5$

behavior as shown in the time series Figure (5.16). The trajectories start to divert at around 75sec.

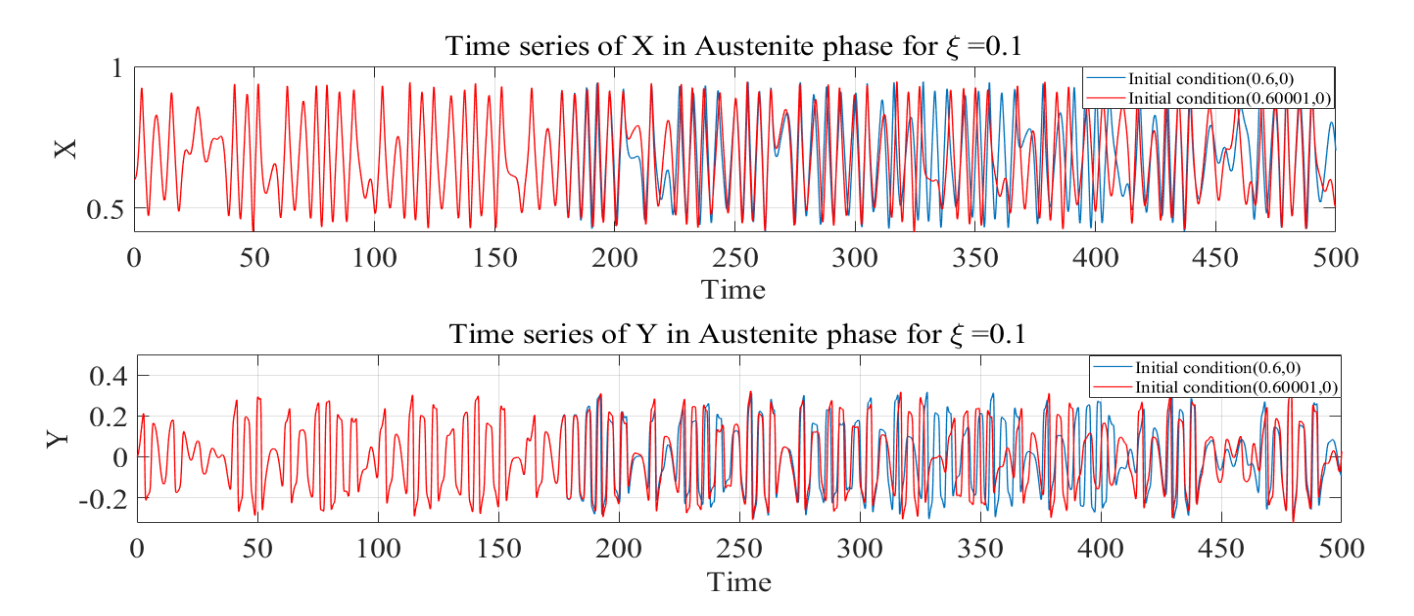


Figure 5.16: Time series for $\xi = 0.1$, showing sensitivity to initial conditions

The Lyapunov exponent for $\xi = 1.5$ is a negative number, which shows the system's convergence behavior as shown in the time series Figure (5.17).

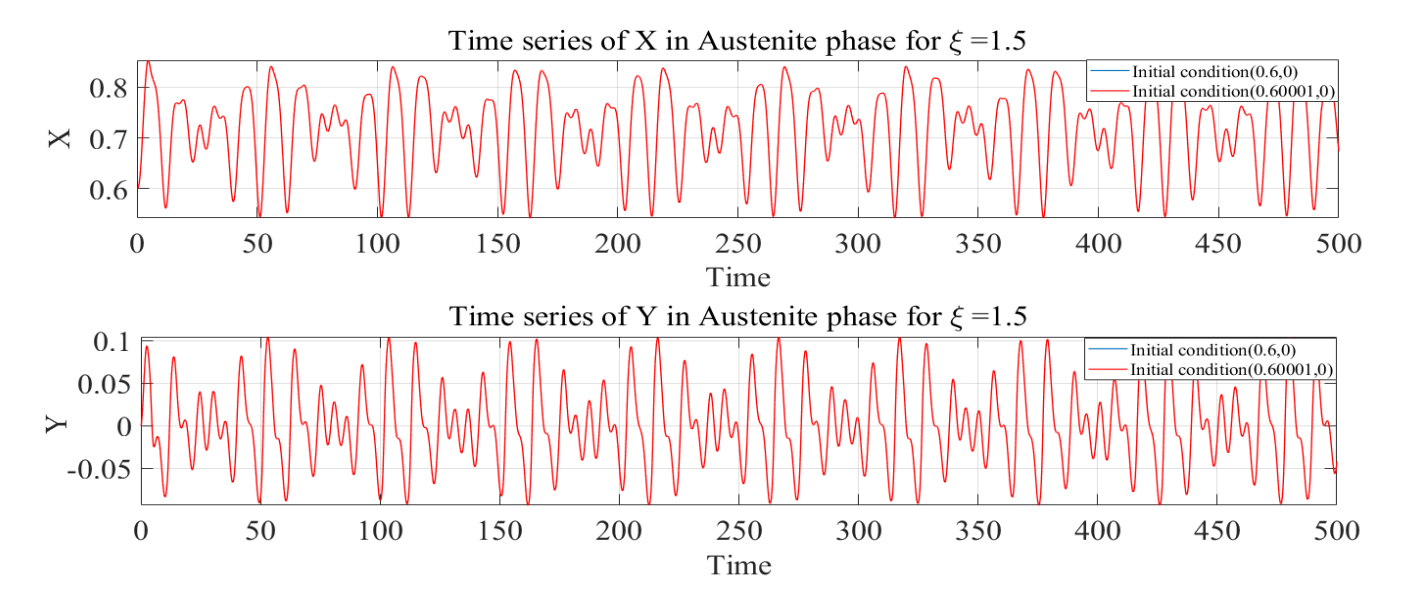


Figure 5.17: Time series for $\xi = 1.5$, showing convergence to initial conditions

However, looking at the forward and backward continuation bifurcation diagram at the austenite phase also shows bistability as stated in Figure (5.18).

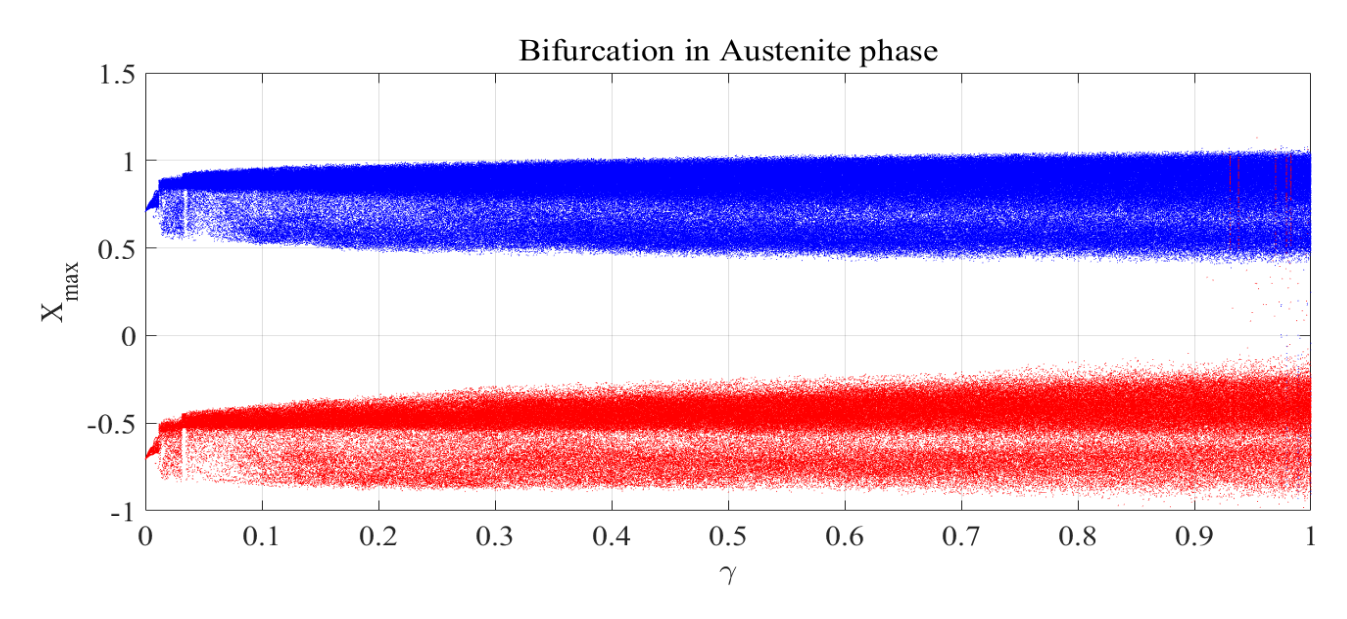


Figure 5.18: Bifurcation in Austenite phase for $\xi = 1.5$

5.6 Adaptive Fuzzy Sliding Mode Controller

The Adaptive Fuzzy Sliding Mode Controller (AFSMC), proposed by Bessa et al.[42], effectively reduces vibrations caused by unknown disturbances. It employs a combination of fuzzy logic and sliding mode control techniques to handle uncertainties in nonlinear systems. By adaptively adjusting its parameters, AFSMC demonstrates superior performance compared to the conventional Sliding Mode Controller (SMC).

The parameters k, λ , and ϕ are crucial in AFSMC's operation. $k = 0.67 + \hat{d}$, λ is a gain which is set to 1, and ϕ is a parameter that decreases the chattering in the SMC. The desired input considered is $[x_d, y_d] = [0, 0]$, aligning with the controller's objective to reduce vibrations in the tripod structure.

To handle the complexity of the system and reduce computational burden, AFSMC employs a combination of triangular and trapezoidal membership functions in its adaptive fuzzy system. These functions, depicted in Figure 5.19, efficiently represent the system's behavior and facilitate accurate estimation of disturbances.

The adaptive fuzzy system accurately approximates the unknown disturbance, which, in this case, exhibits quasi-periodic behavior with three terms excitation. Figure 5.20 illustrates the estimation process, showcasing the system's ability to closely match the actual disturbance profile.

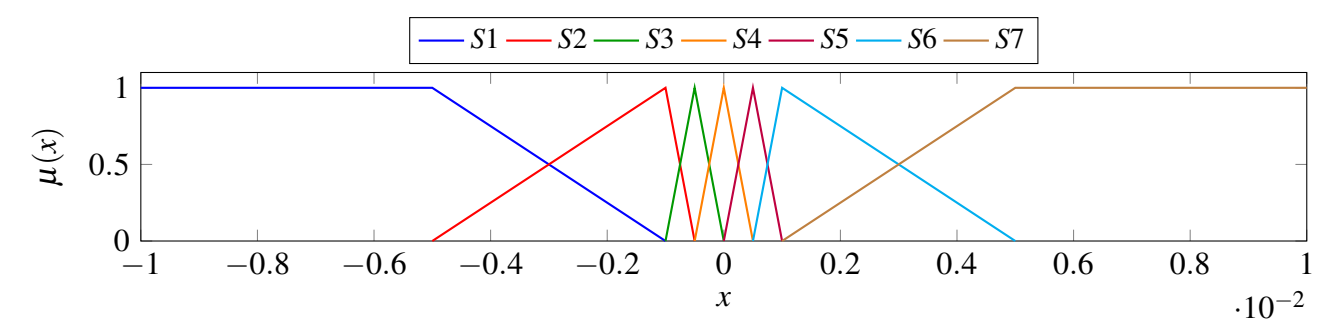


Figure 5.19: Membership Function for the adaptive fuzzy



Figure 5.20: Estimation of disturbance using Adaptive Fuzzy System

The effectiveness of AFSMC is further demonstrated through its performance across different phases of the system: martensite, transition, and austenite.

5.6.1 Martensite phase

In the martensite phase, AFSMC performs well, as shown in Figure (5.21). The controller effective-ly reduces overshoot and undershoot, achieving a quick response time. Table 5.1 further confirms the controller's effectiveness with minimal overshoot and undershoot. A comparison with SMC in Figure (5.22) and Table 5.2 validates the superiority of AFSMC.

Comparing AFSMC with SMC, as depicted in Figure 5.22 and Table 5.2, reinforces AFSMC's robustness and adaptability. In both transition and austenite phases, AFSMC maintains consistent performance, as shown in Figures 5.23 and 5.25, respectively. The similar performance metrics across phases underscore AFSMC's ability to handle varying system dynamics effectively.

In summary, AFSMC's consistent performance across all phases highlights its robustness and adapt-

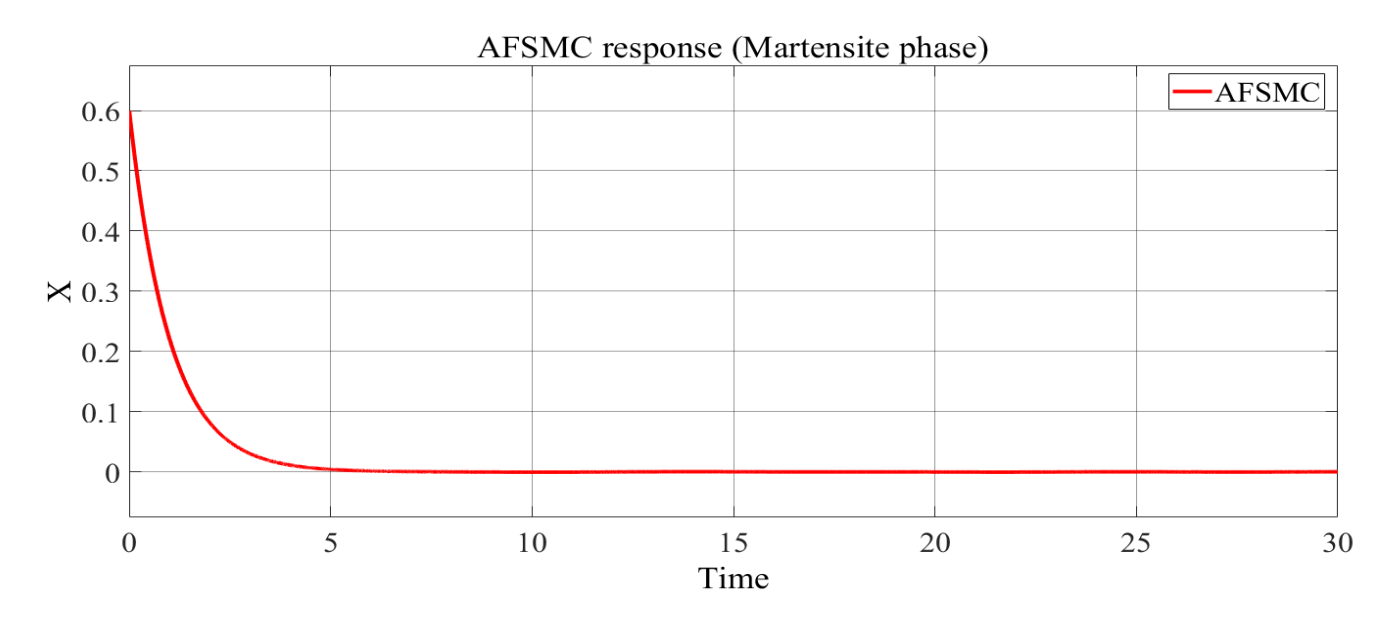


Figure 5.21: AFSMC Performance in Martensite Phase

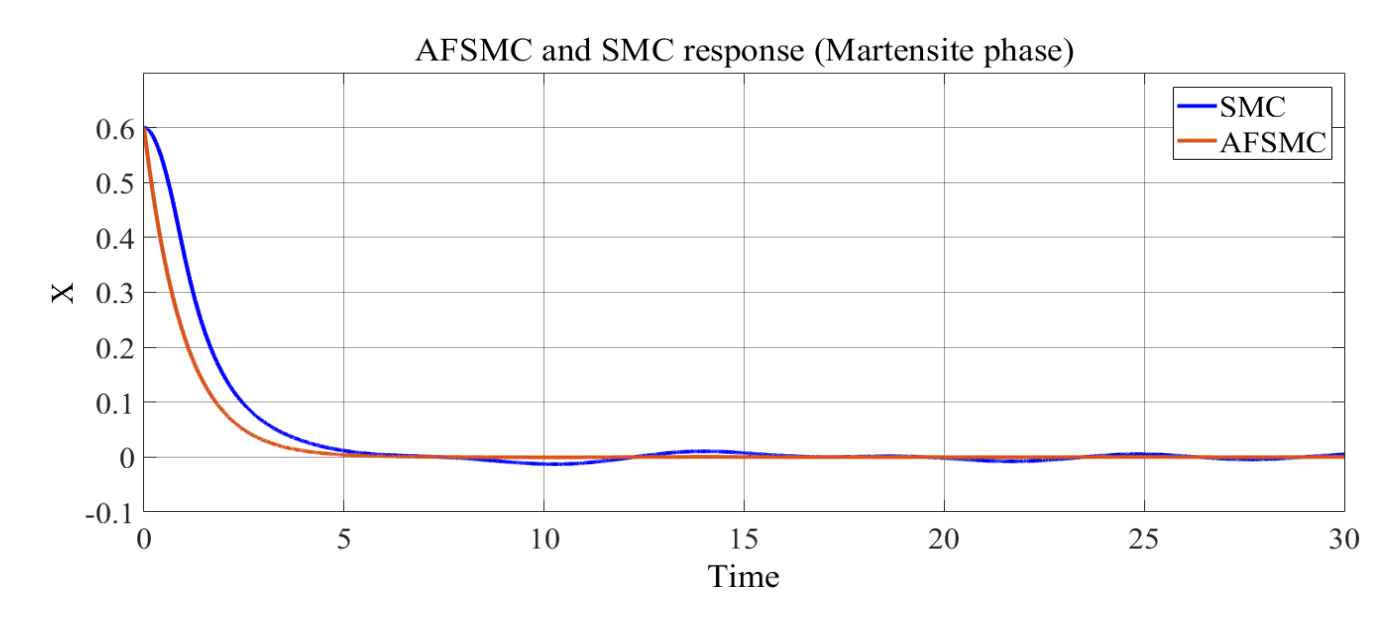


Figure 5.22: Comparison of AFSMC and SMC in Martensite Phase

S.N	Performance Measurement	Value
1	Fall Time	2.133
2	Overshoot	1.995%
3	Undershoot	1.020%
4	ITAE	0.6653
5	IAE	0.6058
6	ISE	0.1808

Table 5.1: AFSMC Controller Performance in Martensite Phase

Measurement	AFSMC	SMC
Fall time	2.133	2.591
Overshoot	1.995%	2.00%
Undershoot	1.020%	2.388%
ITAE	0.6653	2.845
IAE	0.6058	1.034
ISE	0.1808	0.3464

Table 5.2: Comparison of AFSMC and SMC Performance in Martensite Phase

ability in stabilizing the system and reducing vibrations. Its superiority over SMC in terms of fall time, overshoot, and undershoot reaffirms its effectiveness in practical applications.

5.6.2 Transition Phase

In the transition phase, AFSMC maintains consistent performance, as shown in Figure 5.23. The similarity in performance metrics between the martensite and transition phases highlights the robustness of AFSMC across varying system dynamics. Comparative analysis with SMC is presented in Figure 5.24.

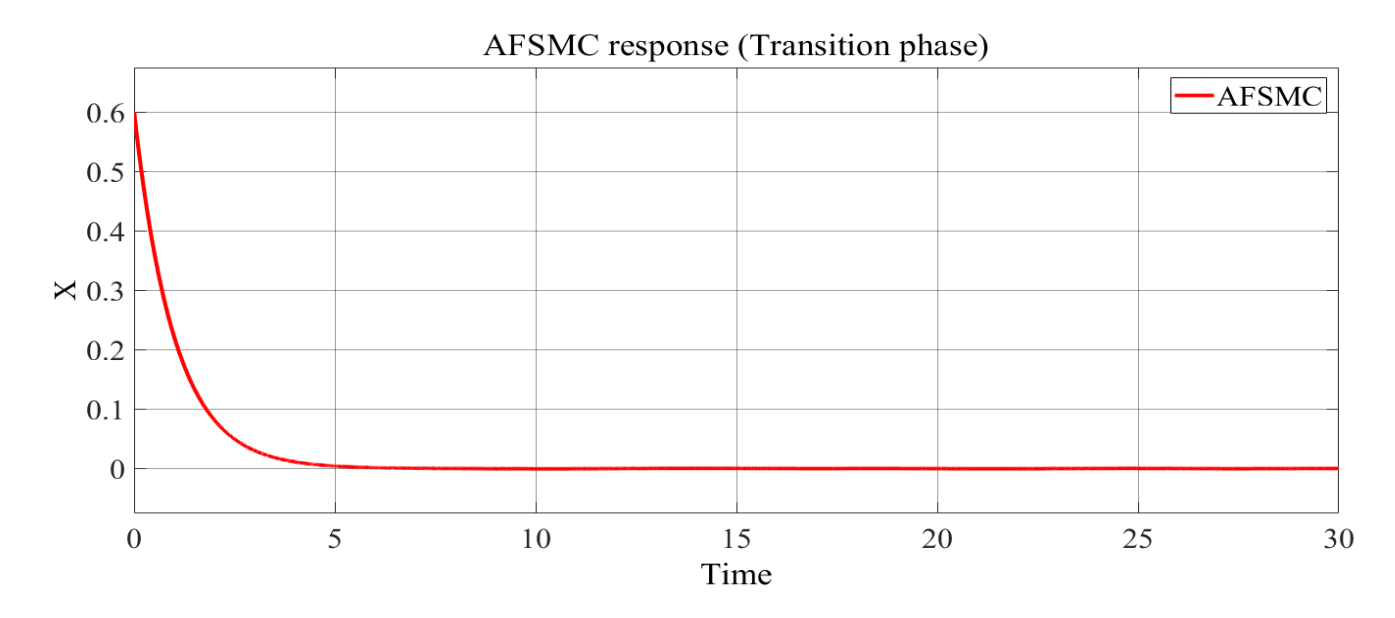


Figure 5.23: AFSMC in Transition Phase

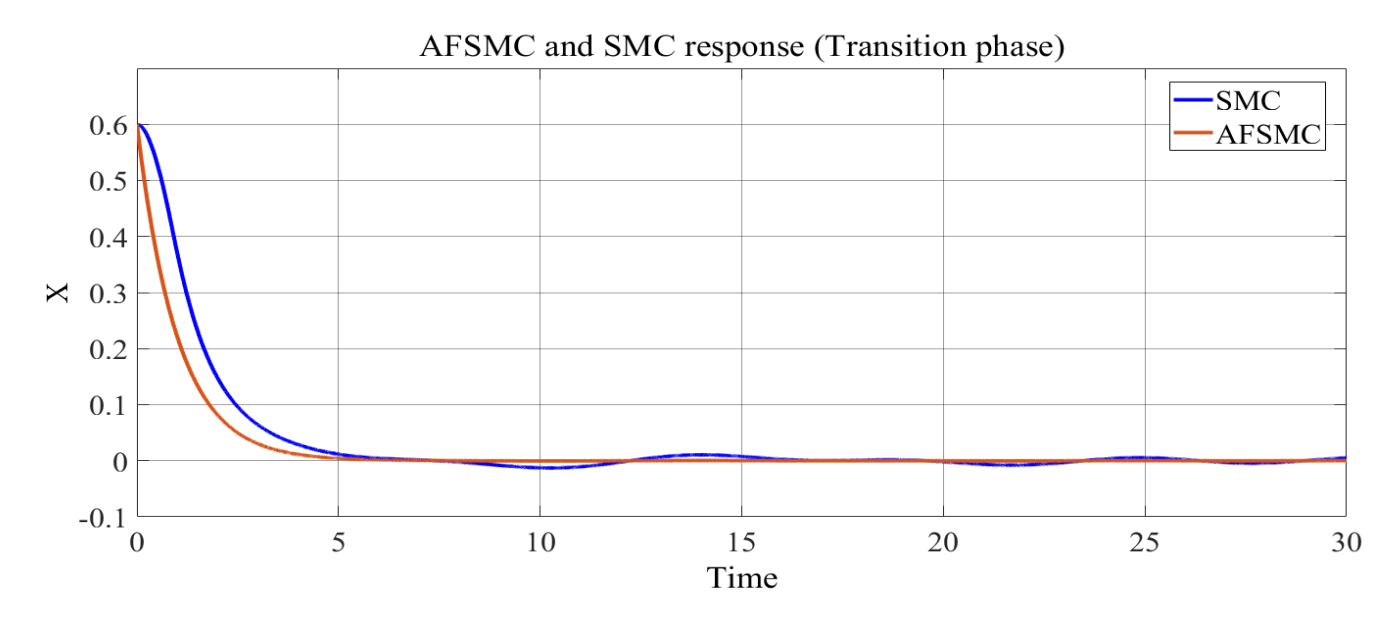


Figure 5.24: Comparison of AFSMC and SMC in Transition Phase

S.N	Performance Measurement	Value
1	Fall Time	2.133
2	Overshoot	1.995%
3	Undershoot	1.020%
4	ITAE	0.6653
5	IAE	0.6058
6	ISE	0.1808

Table 5.3: AFSMC Controller Performance in Transition Phase

Measurement	AFSMC	SMC
Fall time	2.133	2.591
Overshoot	1.995%	2.00%
Undershoot	1.009%	2.388%
ITAE	0.6653	2.845
IAE	0.6058	1.034
ISE	0.1808	0.3464

Table 5.4: Comparison of AFSMC and SMC Performance in Transition Phase

5.6.3 Austenite Phase

AFSMC continues to demonstrate efficacy in the austenite phase, as illustrated in Figure 5.25. The controller achieves rapid settling without significant overshoot or undershoot. Table 5.5 highlights the controller's superiority over SMC.

AFSMC consistently performs well across all phases, indicating its robustness and adaptability in stabilizing the system and reducing vibrations. Its superiority over SMC in terms of fall time, overshoot, and undershoot reaffirms its effectiveness in practical applications.

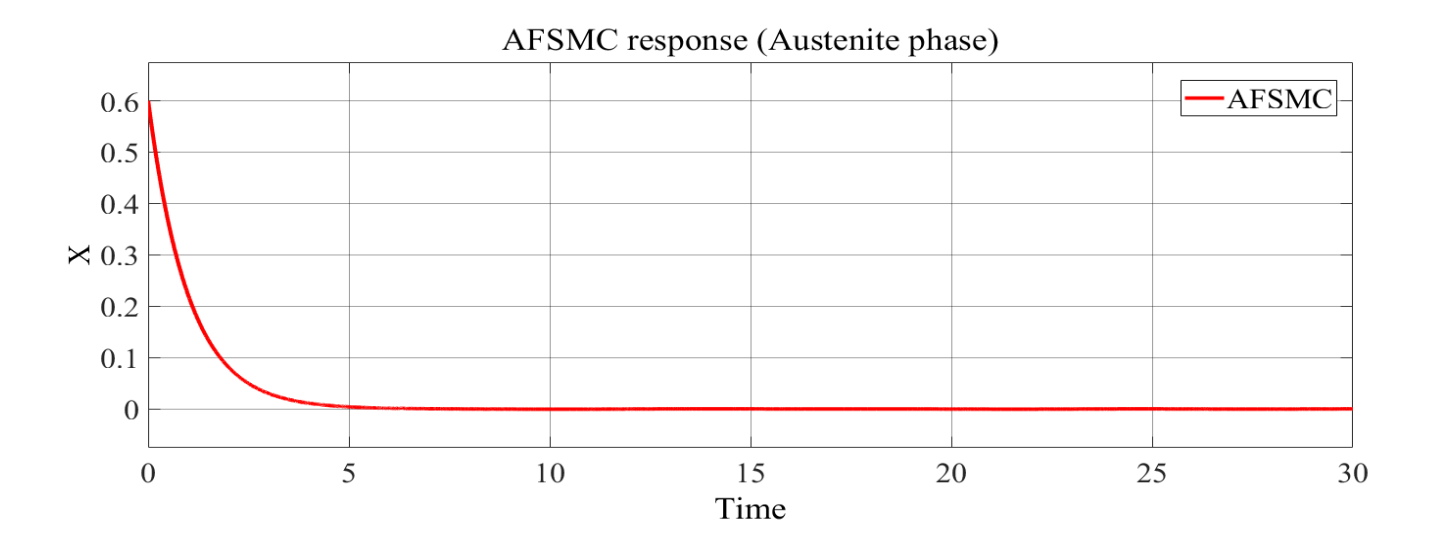


Figure 5.25: AFSMC in Austenite Phase

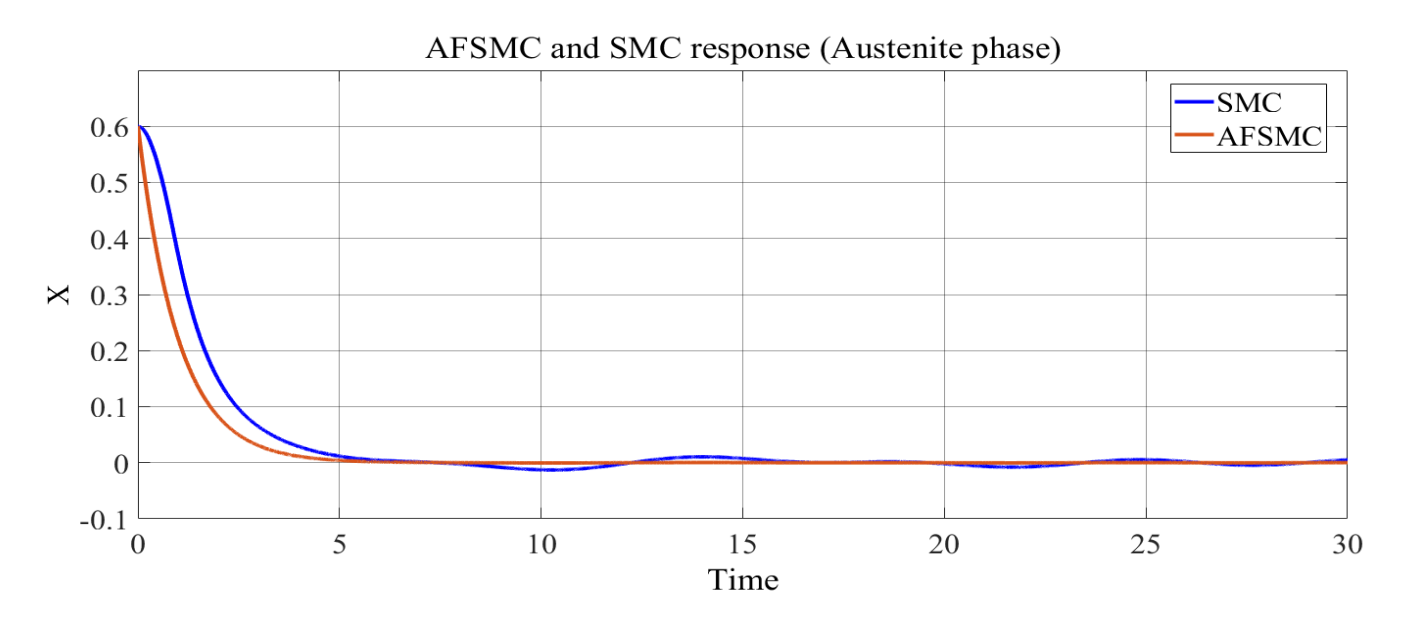


Figure 5.26: Comparison of AFSMC and SMC in Austenite Phase

S.N	Performance Measurement	Value
1	Fall Time	2.133
2	Overshoot	1.995%
3	Undershoot	1.009%
4	ITAE	0.6653
5	IAE	0.6058
6	ISE	0.1808

Table 5.5: AFSMC Controller Performance in Austenite Phase

Measurement	AFSMC	SMC
Fall time	2.133	2.591
Overshoot	1.995%	2.00%
Undershoot	1.009%	2.388%
ITAE	0.6653	2.845
IAE	0.6058	1.034
ISE	0.1808	0.3464

Table 5.6: Comparison of AFSMC and SMC Performance in Austenite Phase

6

Conclusion and Recommendation

6.1 Conclusion

In this study, the non-linear dynamics of a tripod supporter integrated with shape memory alloy (S-MA) is explored and investigated the effectiveness of an Adaptive Fuzzy Sliding Mode Controller (AFSMC) in stabilizing the system across different phases: martensite, transition, and austenite. The analysis provided valuable insights into the behavior of the system under various conditions.

During the martensite phase, it is observed chaotic behavior with $\lambda = 0.2$ under low damping coefficients, while higher damping coefficients led to attracting tori behavior. Bifurcation diagrams illustrated the system's stability for different parameters, indicating bistability with forcing or damping

parameter variations.

In the transition phase, which involves both martensite and austenite phases, it is observed similar dynamics with chaotic behavior with $\lambda=0.18$ under low damping coefficients and attracting tori under higher damping coefficients. Bifurcation diagrams further demonstrated the system's bistability to parameter variations.

In the austenite phase, characterized by high temperatures, the system exhibited chaotic behavior with $\lambda = 0.17$ under small damping coefficients. Still, bistability was observed in this phase.

The AFSMC with parameters $\lambda = 1$, $k = 0.67 + \hat{d}$, and $\phi = 0.1$ showed consistent performance across all phases, effectively reducing overshoot(1.995%) and undershoot(1.020%) while achieving rapid settling. The falltime of AFSMC is 2.134sec. Comparative analysis with the conventional Sliding Mode Controller (SMC) demonstrated the superiority of AFSMC in terms of fall time, overshoot, and undershoot.

Overall, this study highlights the robustness and adaptability of AFSMC in mitigating disturbances and stabilizing the tripod supporter system across different phases.

6.2 Recommendations

Based on the comprehensive analysis conducted in this study, several recommendations can be made to further advance the understanding and application of shape memory alloy (SMA) systems integrated with Adaptive Fuzzy Sliding Mode Control (AFSMC).

Firstly, the study considers the quasi-periodic excitation with three terms of frequency, which describes the complex excitation occurring in real life. However, the system dynamics for random excitation also need to be considered for future works.

Secondly, the system considered in this study is an archetypal model. Thus, it should be correlated with real structures made of shape memory alloy. Additionally, the mechanism of the actuator employed to implement the controller is not considered in this study, presenting a potential avenue for

6.2. Recommendations

future research ideas.

Additionally, the mathematical model employed in this research is developed using integer order method. Mathematical model employing fractional order calculus could be developed to accurately describe the system behaviour.

Moreover, while AFSMC has demonstrated superior performance in reducing vibrations compared to traditional control methods, there is still scope for optimizing its implementation in practical applications. Future research efforts should focus on refining the design and implementation of AFSMC algorithms to enhance their effectiveness and efficiency in real-world scenarios.

In conclusion, by addressing these recommendations, future research endeavors can contribute to advancing the state-of-the-art in SMA-based systems and AFSMC control, ultimately paving the way for their widespread adoption in various engineering applications.

- [1] A. Rao, A. R. Srinivasa, J. N. Reddy, Design of shape memory alloy (SMA) actuators, Vol. 3, Springer, 2015.
- [2] M. K. M. -P. E. N. F. M. N. P. G. Tabrizikahou, Alireza, S. Li., Application and modelling of Shape-Memory Alloys for structural vibration control: State-of-the-art review, Vol. 342, Construction and Building Materials, 2022.
- [3] A. J. Theodore, P. L. Bishay, Experimental analysis of fiber-reinforced laminated composite plates with embedded sma wire actuators, Composite Structures 292 (2022) 115678.
- [4] M. Vollmer, A. Bauer, T. Niendorf, Combined shape memory alloy phenomena: A novel approach to extend applications of shape memory alloys, Materials Letters (2023) 134643.
- [5] F. Falk, Model free energy, mechanics, and thermodynamics of shape memory alloys, Acta Metallurgica 28 (12) (1980) 1773–1780.
- [6] W. Bessa, A. De Paula, M. Savi, Adaptive fuzzy sliding mode control of smart structures, The European Physical Journal Special Topics 222 (7) (2013) 1541–1551.
- [7] M. Varadharajan, P. Duraisamy, A. Karthikeyan, Route to chaos and bistability analysis of quasiperiodically excited three-leg supporter with shape memory alloy, Complexity 2020 (2020) 1– 10.

[8] Y. Tanaka, Y. Himuro, R. Kainuma, Y. Sutou, T. Omori, K. Ishida, Ferrous polycrystalline shape-memory alloy showing huge superelasticity, Science 327 (5972) (2010) 1488–1490.

- [9] D. Canadinc, W. Trehern, J. Ma, I. Karaman, F. Sun, Z. Chaudhry, Ultra-high temperature multi-component shape memory alloys, Scripta Materialia 158 (2019) 83–87.
- [10] V. J. J. P.-S. M. P. I. A. P. V. K. . P. D. M. . P. Chaudhari, R., optimization of wedm process parameters for machining a niti shape memory alloy using a combined approach of rsm and heat transfer search algorithm, Advances in manufacturing 9 (2019) 64–80.
- [11] B. O. G.-X. C. F. T. G. Z. H. G. . . T. T. L. Wheeler, R. W., Engineering design tools for shape memory alloy actuators: Casmart collaborative best practices and case studies., Intelligent Material Systems and Structures 30(18-19) (2019) 2808–2830.
- [12] J. Xia, Y. Noguchi, X. Xu, T. Odaira, Y. Kimura, M. Nagasako, T. Omori, R. Kainuma, Iron-based superelastic alloys with near-constant critical stress temperature dependence, Science 369 (6505) (2020) 855–858.
- [13] G. Costanza, M. E. Tata, Shape memory alloys for aerospace, recent developments, and new applications: A short review, Materials 13 (8) (2020) 1856.
- [14] L. L. H.-Y. C. L. X. S. C. H. W. Z. . . L. Y. Y. Lu, H. Z., Simultaneous enhancement of mechanical and shape memory properties by heat-treatment homogenization of ti2ni precipitates in tini shape memory alloy fabricated by selective laser melting., Materials Science Technology 101 (2020) 205–216.
- [15] K. N. N.-S. A. E. U. A. N. . U. Y. M. Pushin, V. G., Design and development of high-strength and ductile ternary and multicomponent eutectoid cu-based shape memory alloys: Problems and perspectives, Metals 12 (8) (2022) 1289.
- [16] Y. Y. H. Y.-. Y. J. Shen, C., Numerical simulation and experimental comparison of antagonistic shape memory alloy linear actuator for automotive applications, Physics: Conference Series 2383 (1) (2022) 012048.

[17] S. Terrile, A. López, A. Barrientos, Use of finite elements in the training of a neural network for the modeling of a soft robot, Biomimetics 8 (1) (2023) 56.

- [18] R. Liu, C. Zhang, H. Ji, C. Zhang, J. Qiu, Training, control and application of sma-based actuators with two-way shape memory effect, in: Actuators, Vol. 12, MDPI, 2023, p. 25.
- [19] P. Turabimana, J. W. Sohn, S.-B. Choi, A novel active cooling system for internal combustion engine using shape memory alloy based thermostat, Sensors 23 (8) (2023) 3972.
- [20] J. F. Gómez-Cortés, M. L. Nó, A. Chuvilin, I. Ruiz-Larrea, J. M. San Juan, Thermal stability of cu-al-ni shape memory alloy thin films obtained by nanometer multilayer deposition, Nanomaterials 13 (18) (2023) 2605.
- [21] L. Brinson, M. Huang, Simplifications and comparisons of shape memory alloy constitutive models, Journal of intelligent material systems and structures 7 (1) (1996) 108–114.
- [22] S. M. A. B.-A. M. B. . P. P. M. C. L. Paiva, A., A constitutive model for shape memory alloys considering tensile–compressive asymmetry and plasticity, International Journal of Solids and Structures 42 (111-12) (2005) 3439–3457.
- [23] H. Bahrami, S. Hoseini, G. Z. Voyiadjis, Fracture investigation of the shape memory alloy using gtn model, Engineering Fracture Mechanics 216 (2019) 106519.
- [24] C. Yu, G. Kang, Q. Kan, Crystal plasticity based constitutive model of niti shape memory alloy considering different mechanisms of inelastic deformation, International Journal of Plasticity 54 (2014) 132–162.
- [25] K. G. S. Q.-. F. D. Yu, C., Modeling the martensite reorientation and resulting zero/negative thermal expansion of shape memory alloys, Journal of the Mechanics and Physics of Solids 127 (2019) 295–331.
- [26] K. M. C. S. A. S.-S. L. R. M. B. T. . C. S. Mostofizadeh, P., Fatigue analysis of shape memory alloys by self-heating method, International Journal of Mechanical Sciences 156 (2019) 329– 341.

[27] F. R. Phillips, R. W. Wheeler, A. B. Geltmacher, D. C. Lagoudas, Evolution of internal damage during actuation fatigue in shape memory alloys, International Journal of Fatigue 124 (2019) 315–327.

- [28] H. Kiros, Analysis of nonlinear dynamic structures, Momona Ethiopian Journal of Science 6 (1) (2014) 120–130.
- [29] K. Rajagopal, P. Duraisamy, R. Weldegiorgis, A. Karthikeyan, Multistability in horizontal platform system with and without time delays, Shock and Vibration 2018 (2018) 1–8.
- [30] A. S. de Paula, M. A. Savi, Controlling chaos in a nonlinear pendulum using an extended timedelayed feedback control method, Chaos, Solitons & Fractals 42 (5) (2009) 2981–2988.
- [31] e. a. de Paula, Aline S., Controlling a shape memory alloy two-bar truss using delayed feedback method, International Journal of Structural Stability and Dynamics 14 (8) (2014) 1076–1089.
- [32] Z. Huang, C. Du, Y. Li, Bifurcation and chaos of a shape memory alloy supporter, in: 2008 7th World Congress on Intelligent Control and Automation, IEEE, 2008, pp. 8222–8227.
- [33] M.-F. Danca, N. Kuznetsov, Matlab code for lyapunov exponents of fractional-order systems, International Journal of Bifurcation and Chaos 28 (05) (2018) 1850067.
- [34] Y.-J. Liu, Y.-Q. Zheng, Adaptive robust fuzzy control for a class of uncertain chaotic systems, Nonlinear dynamics 57 (3) (2009) 431–439.
- [35] K. Rajagopal, P. Duraisamy, R. Weldegiorgis, A. Karthikeyan, No chattering and adaptive sliding mode control of a fractional-order phase converter with disturbances and parameter uncertainties, Complexity 2018 (2018) 1–8.
- [36] W. M. Bessa, S. Otto, E. Kreuzer, R. Seifried, An adaptive fuzzy sliding mode controller for uncertain underactuated mechanical systems, Journal of Vibration and Control 25 (9) (2019) 1521–1535.
- [37] W. M. Bessa, A. S. de Paula, M. A. Savi, Sliding mode control with adaptive fuzzy dead-zone compensation for uncertain chaotic systems, Nonlinear Dynamics 70 (2012) 1989–2001.

[38] T.-C. Lin, T.-Y. Lee, Chaos synchronization of uncertain fractional-order chaotic systems with time delay based on adaptive fuzzy sliding mode control, IEEE Transactions on Fuzzy Systems 19 (4) (2011) 623–635.

- [39] A. S. De Paula, M. A. Savi, Comparative analysis of chaos control methods: A mechanical system case study, International Journal of Non-Linear Mechanics 46 (8) (2011) 1076–1089.
- [40] S. H. Strogatz, Nonlinear dynamics and chaos: with applications to physics, biology, chemistry, and engineering, CRC press, 2018.
- [41] D. P. Balcerzak, Marek, A. Dabrowski, The fastest, simplified method of lyapunov exponents spectrum estimation for continuous-time dynamical systems, Nonlinear Dynamics 222 (94) (2018) 3053–3065.
- [42] T.-Z. Wu, Y.-T. Juang, Adaptive fuzzy sliding-mode controller of uncertain nonlinear systems, ISA transactions 47 (3) (2008) 279–285.

Appendices



Matlab code for calculating and ploting Equilibrium points and Eigenvalue

Listing A.1: MATLAB code

```
clear all; clc; close all
syms x1 x2
xi = 0.1;
alpha2=124;
alpha3=14505;
gamma=0.045;
b = 0.707;
theta=0.69;
[solx1, solx2] = solve(x2 ==0, (-xi * x2 +
x1 * ((-theta + 1 + (3 * alpha2) - (5 * alpha3)) +
 (theta - 1 - alpha2 + alpha3) * (x1^2 + b^2)^(-1/2) -
 (3 * alpha2 - 10 * alpha3) * (x1^2 + b^2)^(1/2) +
(alpha2 - 10 * alpha3) * (x1^2 + b^2)
 + 5 * alpha3 * (x1^2 + b^2)^(3/2) -
  alpha3 * (x1^2 + b^2)^2) ==0, x1, x2);
x1val = vpa(solx1);
x2val = vpa(solx2);
```

```
E1 = [x1val(1,:); x2val(1,:)];
E2 = [x1val(2,:); x2val(2,:)];
figure();
scatter(E1(1,:), E1(2,:),'filled');
hold on;
scatter(E2(1,:), E2(2,:),'filled');
xlabel('x'); ylabel('y');
legend('E_1','E_2');
title('Equilibrium point');
J = jacobian([x2, (-xi * x2 +
x1 * ((-theta + 1 + (3 * alpha2) - (5 * alpha3))
+ (theta - 1 - alpha2 + alpha3) * (x1^2 + b^2)(-1/2)
  - (3 * alpha2 - 10 * alpha3) * (x1^2 + b^2)^(1/2)
   + (alpha2 - 10 * alpha3) * (x1^2 + b^2)
  + 5 * alpha3 * (x1^2 + b^2)^(3/2) -
    alpha3 * (x1^2 + b^2)^2)), [x1, x2];
J1 = subs(J, \{x1, x2\}, \{E1(1,:), E1(2,:)\});
eigE1=vpa(eig(J1));
J2 = subs(J, \{x1, x2\}, \{E2(1,:), E2(2,:)\});
eigE2=vpa(eig(J2));
figure();
axis equal;
axis([-7, 7, -7, 7]);
xlabel('Real_axis', 'Fontsize', 12);
 ylabel('Img⊔axis', 'Fontsize', 12); grid;
hold on;
plot(real(eigE1(1,:)), imag(eigE1(1, :)), 'bp',
real(eigE1(2,:)), imag(eigE1(2, :)), 'bp');
plot(real(eigE2(1,:)), imag(eigE2(1, :)),
 'rp', real(eigE2(2,:)), imag(eigE2(2, :)), 'rp');
line([0 0], ylim, 'Color', 'black', 'Linewidth', 1);
line(xlim, [0 0], 'Color', 'black', 'Linewidth', 1);
title('Eigen_Values_of_the_equilibrium_points');
```



Matlab code for ploting forward and backward continuation Bifurcation diagram

Listing B.1: MATLAB code

```
% Clear workspace
clear
clear global
% Define global variables
global gamma xi theta alpha2 alpha3 Omega1 Omega2 Omega3 b
xi = 1.5;
%gamma = 0.045;
alpha2 = 124;
alpha3 = 14505;
Omega1 = 0.5;
0mega2 = 0.618;
0mega3 = 1.18;
b = 0.707;
theta = 0.69;
% Simulation step
dt = 1;
% Set initial conditions
```

```
x0 = [0.6, 0];
% Parameter range of interest
stepinterval = 0:0.0003:1;
stepinterval1 = 1:-0.0003:0;
% Presave a matrix of NaNs
M = NaN * zeros(1000, length(stepinterval));
pos = 0;
% Set ode options
options = odeset('RelTol',1e-5,'AbsTol',1e-5);
% Loop over parameter range
for gamma = stepinterval
    gamma
    pos = pos + 1;
    % Simulate the system
    [t, x] = ode45(@tripod_newbif, 0:dt:1000, x0, options);
    % Discard transient
    index = t > 400;
    X = x(index, :);
    % Find local maxima
    P = findpeaks(X(:, 1));
    M(1:length(P), pos) = P;
end
% Presave a matrix of NaNs for the second range
M1 = NaN * zeros(1000, length(stepinterval1));
pos1 = 0;
x0 = x(end,:);
% Loop over the second parameter range
for gamma = stepinterval1
    gamma
    pos1 = pos1 + 1;
    % Simulate the system
    [t, x] = ode45(@tripod_newbif, 0:dt:1000, x0, options);
    % Discard transient
    index = t > 700;
    X = x(index, :);
```

```
% Find local maxima
P = findpeaks(X(:, 1));

M1(1:length(P), pos1) = P;
end

% Plot the result
hold on
plot(stepinterval, M, '.b', 'MarkerSize', 2) % Changed color to blue
plot(stepinterval1, M1, '.r', 'MarkerSize', 2) % Plotted the second range in red
xlabel('\xi')
ylabel('max(x)')
set(gca, 'fontsize', 12)
set(gca, 'fontweight', 'bold')
box on
```



Matlab code for implementing the adaptive fuzzy system

Listing C.1: MATLAB code

```
function d_hat_s = adaptiveFuzzyLogic(s)
    % Define membership functions
    function S = openleft(x, a, b)
        if x < a
            S = 1;
        elseif a < x & x < b
            S = (x - a) / (b - a);
        else
            S = 0;
        end
    end
    function S = openright(x, a, b)
        if x < a
            S = 0;
        elseif a < x & x < b
            S = (x - a) / (b - a);
        else
            S = 1;
        end
```

```
end
function S = triangular(x, a, b, c)
    \mathtt{if} \ \mathtt{x} \ < \ \mathtt{a}
        S = 0;
    elseif a < x & x < b
        S = (x - a) / (b - a);
    elseif b < x & x < c
        S = (c - x) / (c - b);
    else
        S = 0;
    end
end
% Define partition function
function [S1, S2, S3, S4, S5, S6, S7] = partition(x)
    S1 = openleft(x, -0.007, -0.001);
    S2 = triangular(x, -0.005, -0.001, -0.0005);
    S3 = triangular(x, -0.001, -0.0005, 0);
    S4 = triangular(x, -0.0005, 0, 0.0005);
    S5 = triangular(x, 0, 0.0005, 0.001);
    S6 = triangular(x, 0.0005, 0.001, 0.005);
    S7 = openright(x, 0.001, 0.007);
end
% Partition the input value s
[S1, S2, S3, S4, S5, S6, S7] = partition(s);
% Define adaptive parameters
% Initialize D vector with zeros (column vector)
D_{initial} = zeros(7, 1);
phi = 0; % Adaptation rate constant
% Compute Psi(s)
w = [S1, S2, S3, S4, S5, S6, S7];
if sum(w) \sim 0
    Psi_s = w / sum(w);
    % Define parameters for the ODE solver
     % Adjust tolerance
    options = odeset('RelTol', 1e-6, 'AbsTol', 1e-9);
    tspan = [0, 1000]; % Define the initial and final time
    % Call the ODE solver
    [", D] = ode45(@(t, D) myODE(t, D, s, Psi_s, phi), tspan, D_initial, options);
    % Compute the weighted average output d_hat(s)
```